AD-A177 003 FLUID DYNAMICS OF HIGH PERFORMANCE TURBOMACHINES(U) 1/1
MASSACHUSETTS INST OF TECH CAMBRIDGE GAS TURBINE LAB
E M GREITZER ET AL NOV 86 AFOSR-TR-87-0038
UNCLASSIFIED F49620-85-C-0018 F/G 13/7 NL

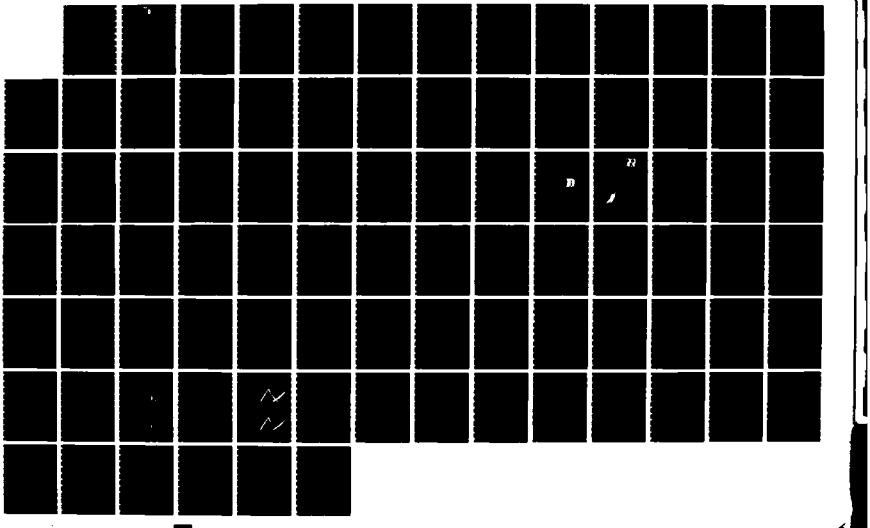

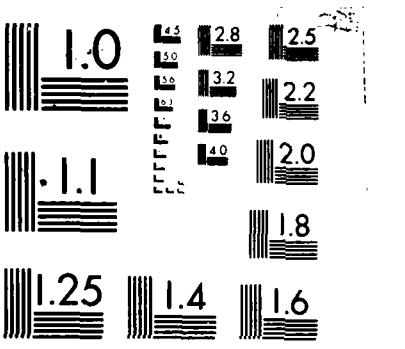

RITY CLASSIFICATION OF THIS PAGE

(21)

UNCLASSIFIED

REPORT DOCUMENTATION PAGE

DTIC ELECTE FEB 25 1987 D

AD-A177 003

	1b. RESTRICTIVE MARKINGS: None
HEDULE	3. DISTRIBUTION/AVAILABILITY OF REPORT: Approved for public release, distribution unlimited
4. PERFORMING ORGANIZATION REPORT NUMBER(S): MASSACHUSETTS INSTITUTE OF TECHNOLOGY	5. MONITORING ORGANIZATION REPORT NUMBER(S): AFOSR-TR- 87-0038
6a. NAME OF PERFORMING ORGANIZATION: Department of Aeronautics and Astronautics	6b. OFFICE SYMBOL (If applicable): 31-264
7a. NAME OF MONITORING ORGANIZATION: AFOSR/NA	
6c. ADDRESS (City, State, and ZIP Code): Cambridge, MA 02139	7b. ADDRESS (City, State, and ZIP Code): BOLLING AFB DC 20332-6448
8a. NAME OF FUNDING/SPONSORING ORGANIZATION: AFOSR	8b. OFFICE SYMBOL (If applicable): AFOSR.NA
9. PROCUREMENT INSTRUMENT IDENTIFICATION NUMBER: Contract F49620-85-C-0018	
8c. ADDRESS (City, State, and ZIP Code): AFOSR Bolling AFB, DC 20332	10. SOURCE OF FUNDING NUMBERS: PROGRAM ELEMENT NO. 61102F; PROJECT NO. 2307; TASK NO. A1; WORK UNIT ACCESSION NO.

11. TITLE (Include Security Classification): Fluid Dynamics of High Performance Turbomachines

12. PERSONAL AUTHOR(S): E.M. Greitzer, A.H. Epstein, M.B. Giles, J.E. McCune, C.S. Tan

13a. TYPE OF REPORT	13b. TIME COVERED	14. DATE OF REPORT (Year, Month, Day)	15. PAGE COUNT
Annual	FROM 10/19/85 TO 10/18/86	11/24/86	85

16. SUPPLEMENTARY NOTATION

17. COSATI CODES		
FIELD	GROUP	SUB-GROUP

18. SUBJECT TERMS (Continue on reverse if necessary and identify by block number): Transonic Compressors; Compressor Stability; Casing Treatment Design; Vortex Wakes; Unsteady Flows in Turbomachines.

19. ABSTRACT (Continue on reverse if necessary and identify by block number)

This report gives a summary of work carried out at the Gas Turbine Laboratory at MIT, during the period 10/19-85 to 10/18/86, as part of our multi-investigator effort on high performance turbomachinery fluid dynamics. Within the general topic, four separate tasks are specified. These are, in brief: I. Loss mechanisms and loss migration in transonic compressors, including development of advanced instrumentation for measurements of wake radial transport and analysis of unsteady vortical wake structures. II. Experimental and theoretical study of flows in casing and hub treatment, including mechanisms for stability enhancement in compressors and unsteady fluid dynamic interactions between passage and groove flows. III. Computational techniques for turbomachinery, including inverse (design) calculation procedures for transonic turbomachine blades accounting for viscid/inviscid interaction. IV. Theoretical modelling of stability and unsteadiness in transonic compressor flow fields, including analyses of unsteady temperature fluctuations due to vortex shedding.

FILE COPY

20. DISTRIBUTION/AVAILABILITY OF ABSTRACT	21. ABSTRACT SECURITY CLASSIFICATION
☐ UNCLASSIFIED/UNLIMITED ☒ SAME AS RPT ☐ DTIC USERS	UNCLASSIFIED

22a. NAME OF RESPONSIBLE INDIVIDUAL	22b. TELEPHONE (Include Area Code)	22c. OFFICE SYMBOL
DR JAMES D WILSON	202-767-4935	AFOSR/NA

DD FORM 1473, 84 MAR — 83 APR edition may be used until exhausted. All other editions are obsolete.

SECURITY CLASSIFICATION OF THIS PAGE

UNCLASSIFIED

GAS TURBINE LABORATORY
DEPARTMENT OF AERONAUTICS AND ASTRONAUTICS
MASSACHUSETTS INSTITUTE OF TECHNOLOGY
CAMBRIDGE, MA 02139

ANNUAL TECHNICAL REPORT

on

CONTRACT NO. F49620-85-C-0018

entitled

FLUID DYNAMICS OF HIGH PERFORMANCE TURBOMACHINES

for the period

October 19, 1985 to October 18, 1986

submitted to

AIR FORCE OFFICE OF SCIENTIFIC RESEARCH

Attention: Dr. James Wilson, Program Manager
AFOSR/NA
Directorate of Aerospace Sciences
Building 410
Bolling Air Force Base, DC 20332

Principal Investigator: Edward M. Greitzer
Professor and Director, Gas Turbine Laboratory

Co-Investigators: Prof. Alan H. Epstein
Prof. Michael B. Giles
Prof. James E. McCune
Dr. Choon S. Tan

November 1986

TABLE OF CONTENTS

1. INTRODUCTION AND RESEARCH OBJECTIVES

This report describes work carried out at the Gas Turbine Laboratory at MIT, as part of our multi-investigator effort on high performance turbomachinery fluid dynamics. Support for this program is provided by the Air Force Office of Scientific Research under Contract Number F49620-85-C-0018, Dr. J.D. Wilson, Program Manager.

The present report gives a short summary of the work for the period 10/19/85 - 10/18/86. For further details and background, the referenced laboratory reports, publications, the previous final report (Reference 1) covering the period 10/1/81 - 9/30/84, and the two recent progress reports on the current contract should be consulted.

Within the general topic, four separate tasks are specified. These are, in brief:

I. Loss mechanisms and loss migration in transonic compressors, including development of advanced instrumentation for measurements of wake radial transport and analysis of unsteady vortical wake structures.

II. Experimental and theoretical study of flows in casing and hub treatment, including mechanisms for stability enhancement in compressors and unsteady fluid dynamic interactions between passage and groove flows.

III. Computational techniques for turbomachinery, including inverse (design) calculation procedures for transonic turbomachine blades accounting for viscid/inviscid interaction.

IV. Theoretical modelling of stability and unsteadiness in transonic compressor flow fields, including analyses of unsteady temperature fluctuations due to vortex shedding.

The work carried out in each of the tasks will be described in the next section.

References

1. E.M. Greitzer, et al., Final Report, 10/81 - 9/84, on "Current Problems in Turbomachinery Fluid Dynamics."

2. E.M. Greitzer, A.H. Epstein, M.B. Giles, J.E. McCune, C.S. Tan, Annual Technical Report on Contract F49620-85-C-0018, "Fluid Dynamics of High Performance Turbomachines," November 1985.

3. E.M. Greitzer, A.H. Epstein, M.B. Giles, J.E. McCune, C.S. Tan, Research Progress and Forecast Report on Contract F49620-85-C-0018, "Fluid Dynamics of High Performance Turbomachines," March 1986.

TASK I: LOSS MECHANISMS AND LOSS MIGRATION IN TRANSONIC COMPRESSORS

Objectives

The primary objective of this effort is to elucidate and quantify the physical mechanisms which produce loss (entropy) in a high speed compressor, with particular attention to three-dimensional and unsteady effects. The motivations for this work are twofold. The first is the desire to dramatically improve the design point performance of high speed compressors to meet the ambitious Air Force propulsion goals of the 1990's. The second is the realization (spurred by AFAPL data showing apparent efficiencies above 100%) that there are important physical phenomena influencing the behavior of compressors which are not at all understood or accounted for in present design methodologies.

Progress During This Year

Effort during the past year has been concentrated in three areas: analysis of the effects of wake structure on compressor efficiency and the interpretation of performance measurements; an ab initio calculation of the unsteady flow in transonic blade rows using a 2-D, time accurate, Reynolds averaged Navier-Stokes procedure; and continued work in the mapping of the radial flow in a transonic compressor rotor.

Wake Structure Effects

The analysis of the effects of wake structure on apparent compressor efficiency is a follow-up to work reported earlier which identified vortex street structures in the wakes of high performance transonic compressors, through both experimental and analytical investigations. It has been shown that a vortex street structure in the compressor wake can influence the compressor efficiency, noise, and structural integrity. The analysis also shows that the wake structure can influence the measurement of compressor performance,

introducing artifacts even with "perfect" instrumentation. For the stage studied here, this measurement error is of the order of 1% in efficiency.

Another interesting effect of the vortex street is to redistribute thermal energy in the compressor, thus introducing total temperature gradients. The total temperature gradients combine with the shock structure in the compressor to yield an unusual result, adiabatic efficiency (the common measure of compressor performance) and entropy change are no longer congruent as they are in flow with uniform total temperature. Thus, our well developed "feel" for these flow field descriptors is erroneous. Although this is really a bookkeeping problem, it may have an important influence in how we design and compare turbomachines.

Numerical Flow Field Simulation

To further investigate compressor wake structure, a 2-D, time accurate, viscous, Reynolds averaged Navier-Stokes calculation of a rotor passage was performed using the midspan geometry of an experimentally investigated compressor. This ab initio calculation, which has a uniform inflow condition, shows vortex shedding very similar to that observed experimentally. The mean frequencies of shedding from the calculation and those inferred from two independent measurement techniques are all about 15 kHz, 3 times the rotor passing frequency, a very strong, mutual confirmation.

A surprising result of the calculation was a low frequency (350 Hz) modulation of vortex shedding, apparently caused by motion of the separation point along the suction surface of the airfoil. This oscillation appears similar in nature to a diffuser instability and was observed (but remained unexplained) in experimental measurements. The importance of this low frequency instability is not fully understood but since a) the resultant total pressure fluctuations are on the order of 5% of the stage pressure rise, and

b) the instability results in a 30% fluctuation in blade moment at a frequency within 5% of the first blade bending frequency, we believe that further investigation is warranted.

Overall, from this work we have made the following observations.

1. The wakes of high Reynolds number, transonic compressor blades can consist of shed vortex streets. This is confirmed by measurement, modelling, and numerical simulation.
2. The vortex shedding scales with wake thickness.
3. The shedding frequency and strength are sensitive to the environment.
4. The vortex street can depress the average wake temperature.
5. The effect of the wake structure on temperature and pressure levels increases with the square of the freestream Mach number.
6. Wake structure can influence the measurement of compressor efficiency.
7. Changes in wake structure can be mistaken for changes in compressor performance.
8. The wake structure can drive the blade shock system, inducing loss.
9. The wake structure can be influenced by other fluid dynamic instabilities present in a blade passage which themselves may be important for performance and structural dynamic reasons.
10. Caution is required when interpreting steady state solutions of inherently unsteady flowfields.

More detail is included in the paper preprint appended.

Radial Flow Migration in a Transonic Rotor

The structure of the radial flows in a turbomachine can have an important influence on the behavior of a given stage as well as on the performance of subsequent blade rows downstream. These radial flows give rise to spanwise mixing which is a key determinant of multistage compressor performance. The

nature of magnitude of this process has recently become a topic of considerable debate (Atkins and Smith versus Gallimore and Cumpsty) fueled by its very real practical importance. In all cases to date, these radial mixing processes have been treated only in the time average. In this work, we are taking time resolved measurements of the flow field using a tracer gas to elucidate the radial flow transport in the rotor. The motivation is both to unsort the radial flow structure (spanwise vortex coherence, flows in boundary layer seapration regions, etc.), and to quantify the radial mixing mechanisms.

The mapping of the radial flow in the AFAPL high thru-flow rotor is being carried out using gas injection in the MIT Blowdown Compressor Facility. Basically, a circumferential sheet of gas (helium) is injected upstream of the rotor and the time resolved concentration distribution of the injectant is measured at the rotor outlet. The experimental technique has been developed during previous years of this effort. The layout of the apparatus is shown in Figs. 1 and 2. The injector was first run in the tunnel without the compressor stage to establish a baseline mixing rate for the injectant sheet. The stage was then run with the injector present, with and without the injectant turned on, to indicate the effect of the injector hardware (blockage and viscous wake) on the stage performance. The experiment with injectant was then run, sample data from which is shown in Fig. 3.

The experiment has proven considerably more difficult than first expected, with detection sensitivity the principal problem. For this reason, the tracer gas has been changed from CO_2 (the best match to the main flow) to helium (ten times the sensitivity). To date, the flow has been mapped with injection at the midspan and hub positions.

It is planned to finish the experimental mapping over the course of the next year and to reduce and model the data. Preliminary analysis shows the time averaged results match those of Gallimore and Cumpsty.

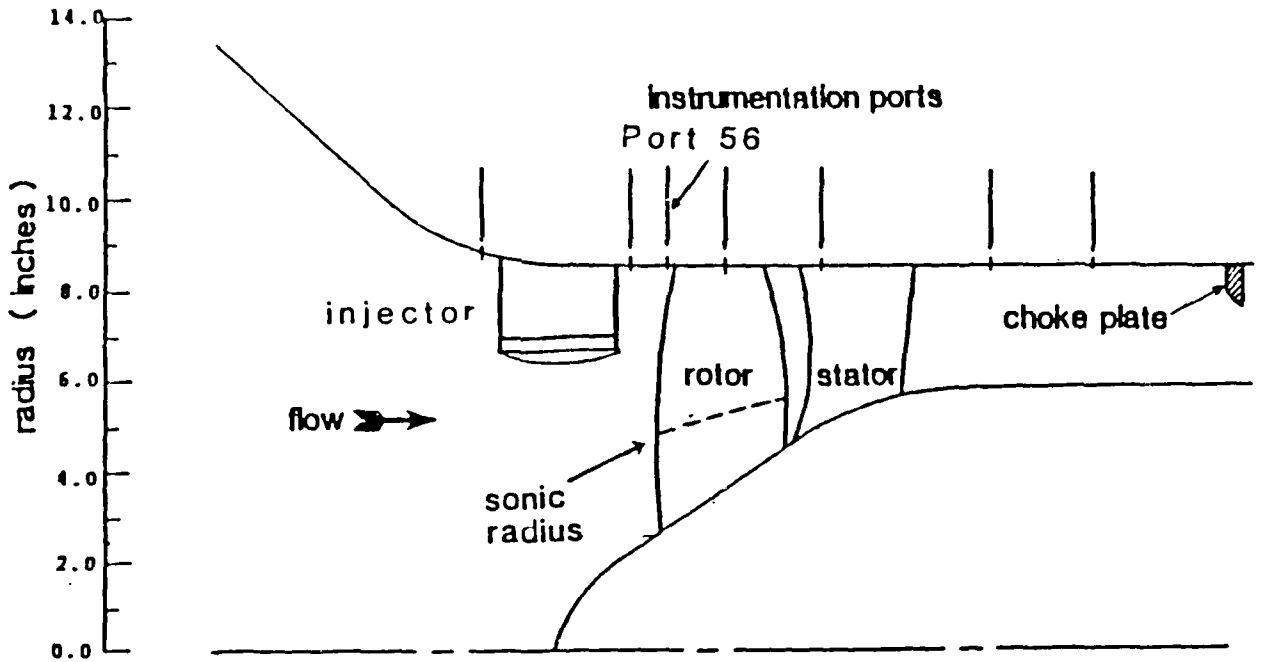

Air Force High Thru Flow Stage (AFAPL)

Figure 1: Scale drawing of the test section

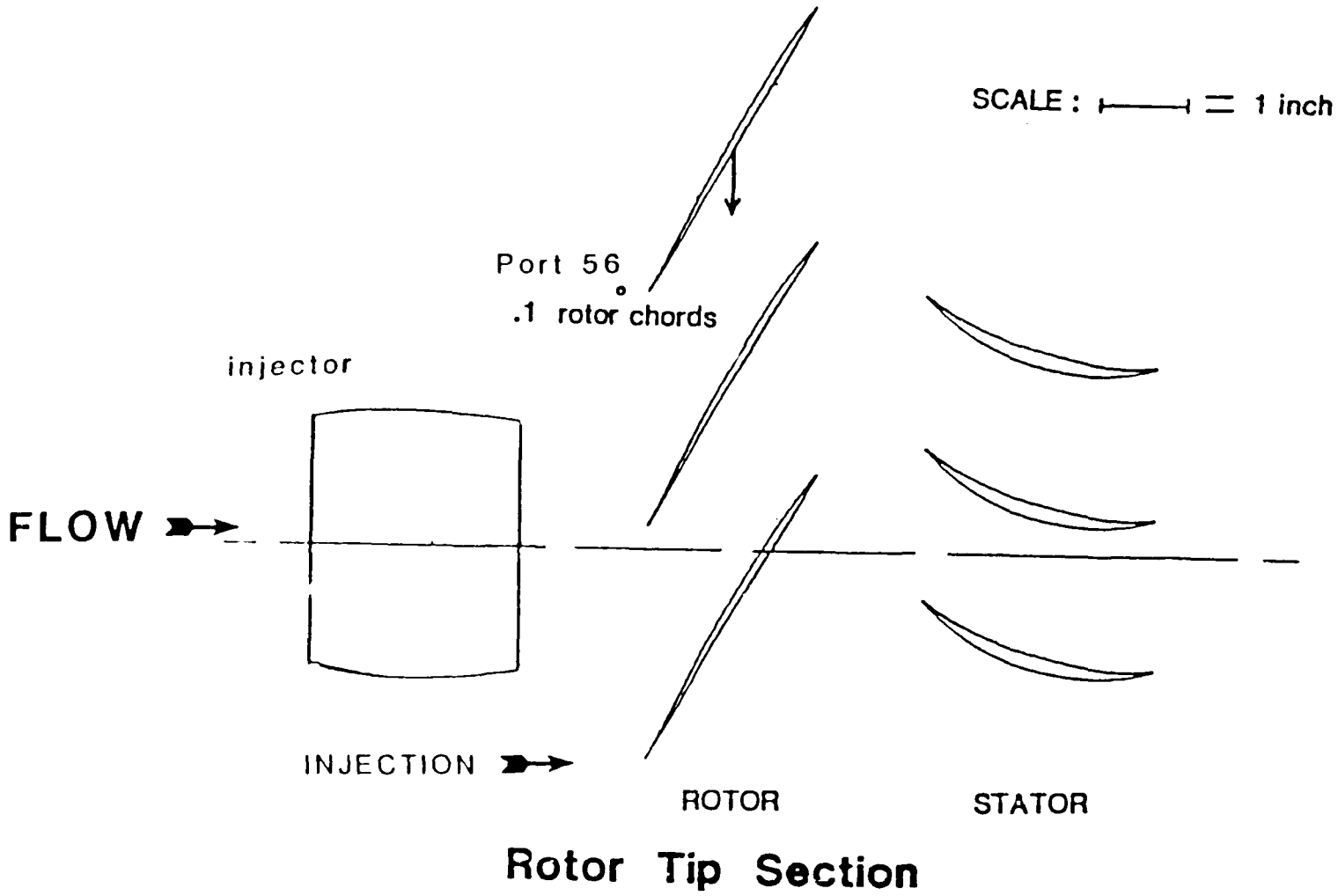

Figure 2: Top view of the experimental arrangement

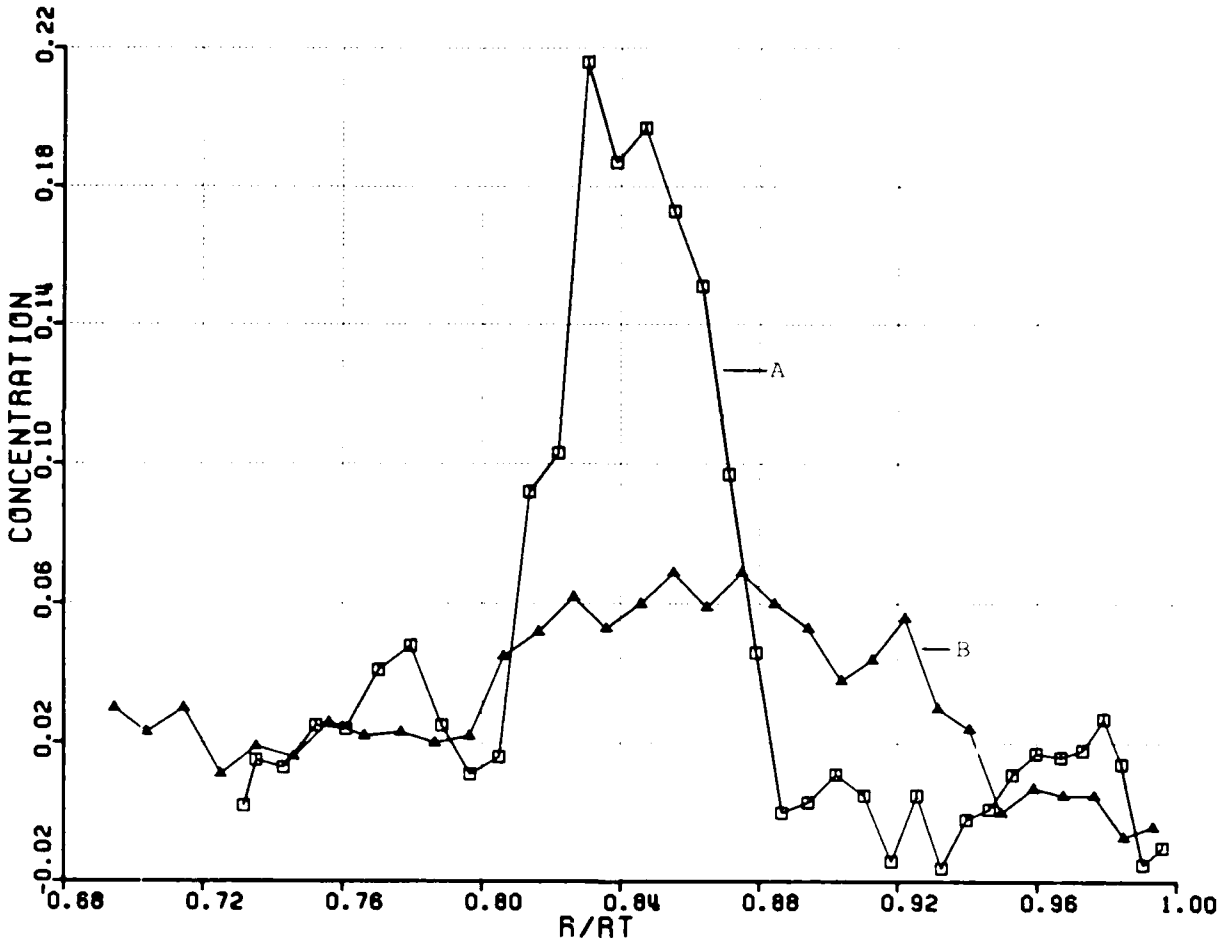

Figure 4a: Time-averaged tracer concentration
A) No injectant
B) Injection at midspan

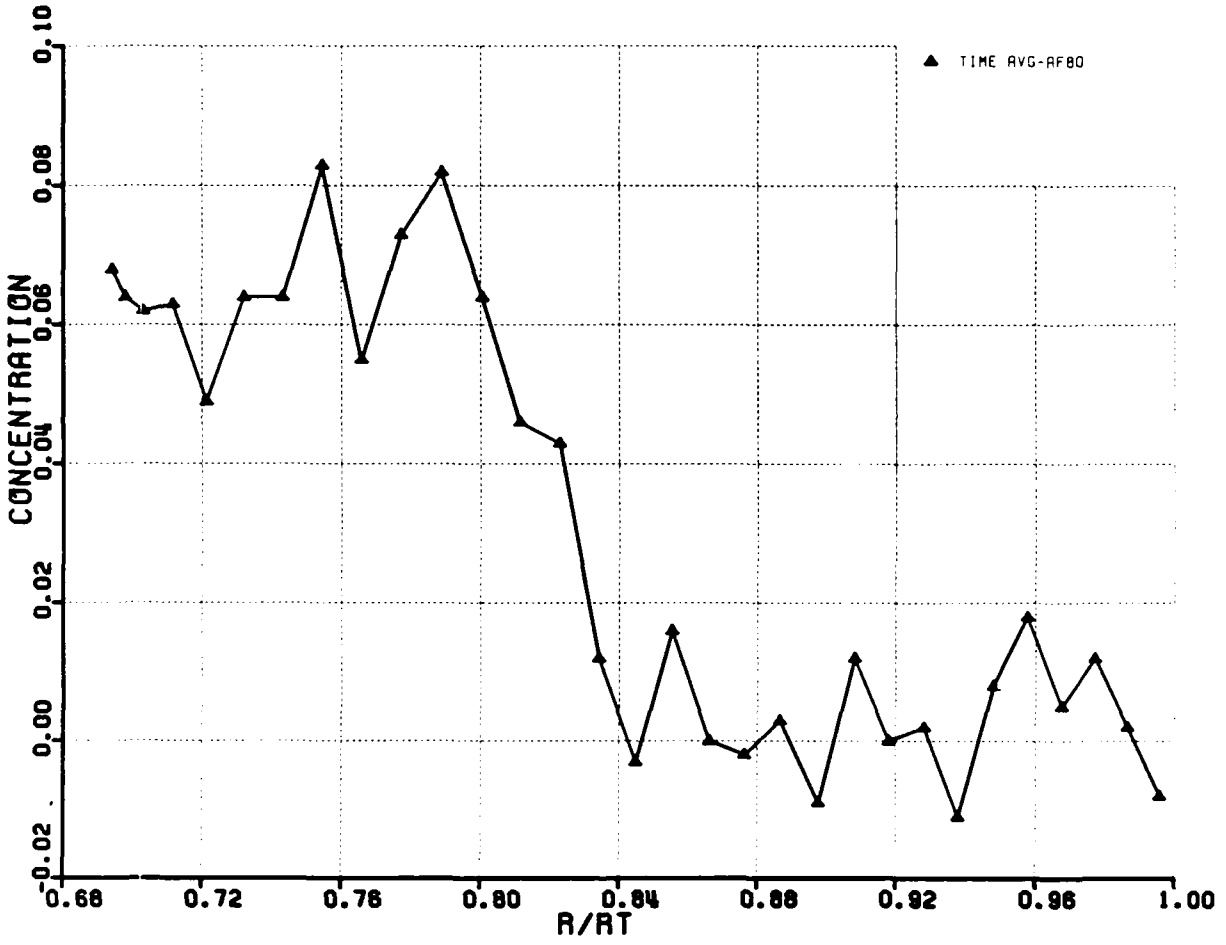

Figure 3b: Time average tracer concentration, injection near hub

VORTEX SHEDDING IN HIGH SPEED COMPRESSOR BLADE WAKES

A.H. Epstein, J.B. Gertz, P.R. Owen and M.B. Giles
Gas Turbine Laboratory
Massachusetts Institute of Technology
Cambridge, MA 02139 USA

ABSTRACT

The wakes of highly loaded compressor blades are generally considered to be turbulent flows. Recent work has suggested that the blade wakes are dominated by a vortex street-like structure. The experimental evidence supporting the wake vortex structure is reviewed. This structure is shown to redistribute thermal energy within the flowfield. The effect of wake structure on conventional aerodynamic measurements of compressor performance is noted. A two-dimensional, time accurate, viscous numerical simulation of the flow exhibits both vortex shedding in the wake and a lower frequency flow instability which modulates the shedding. The numerical results are shown to agree quite well with the measurements from transonic compressor rotors.

1. INTRODUCTION

Although bluff bodies and low speed airfoils have long been known to shed vortices into their wakes, the wakes of high speed, high Reynolds number turbomachinery blading have generally been considered to be turbulent and unstructured. Usually, the wake is described only in terms of a time averaged velocity profile. This is consistent with the view that, assuming uniform inflow and excepting turbulence, the flow in the frame moving with the compressor rotor is uniform and that variations observed in the stationary frame are primarily due to blade to blade geometric differences. This view, however, is erroneous in detail with practical import for compressor design.

There is a considerable body of experimental data which shows that blunt trailing edge airfoils typical to turbines shed vortex streets [1], [2], [3].

Recent work has shown that a similar phenomenon may occur in sharp trailing edge transonic compressors as well [4].

If we assume for the moment that high speed compressor blade wakes can consist of a vortex street-like structure, then a number of questions immediately become relevant. These include: do all blade wakes contain vortices; why are the vortices rarely observed experimentally; how are the vortex streets formed and what is their structure; and what is the practical importance of the wake structure to the compressor designer? We will address the last question first so as to provide a groundwork for the discussions which follow.

In the context of high efficiency, high performance transonic compressors and fans, the influence of the wake temporal and spatial structure for a given time averaged velocity defect can be surprisingly large. The wake structure can influence the compressor aerodynamics, noise, and structural integrity. Vortex shedding decreases the blade row efficiency (higher base drag and shock loss, increased unsteadiness) and induces artifacts in standard measurement techniques. An increased level of unsteadiness into following blade rows can increase the loss there and alter the mass flow characteristics, independently of whether that blade row is itself shedding vortices. The interaction of the shed vortex street with subsequent blade rows is also a source of noise. Obviously, the unsteady loading due to the vortex streets and related phenomena can have deleterious effects on the structural integrity of a compressor when the aerodynamic excitation frequencies coincide with those which are structurally important. The blade wake structure also influences compressor design and analysis in that it represents a physical phenomenon not usually modelled (either because the analysis is inviscid or steady state). Thus, the design intent may not represent a physically realizable system.

This paper is an extension of previous work in which the presence of vortex streets was inferred from experimental measurements and their effect on the blade shock system discussed [4], [5]. Here, we review that work, discuss the effects of vortex streets on the temperature distribution within the flow, note the influence of the wake structure on conventional aerodynamic performance measurements, present the results of an ab initio numerical simulation showing similar behavior, and suggest areas for further investigation.

2. REVIEW OF EXPERIMENTAL OBSERVATIONS

Flow visualization studies have demonstrated the existence of vortex streets in the wakes of transonic flat plate and turbine airfoil cascades [1], [2], [3] but, excepting the special case of acoustic resonance enhanced shedding [6], [7], shedding in high speed compressor airfoils had not been conclusively reported. Hot wire measurements in the wakes of controlled diffusion airfoil cascades yielded ambiguous results [8] with one configuration showing evidence of periodicity in the wake while another did not. In the context of hydrofoils, Blake [9] suggested that all bodies shed but may do so in a discontinuous fashion, i.e., shed in bursts. Lack of phase coherence between the bursts would then tend to obscure the shedding when examined with spectral analysis techniques. This is consistent with the observation that the least ambiguous information has been instantaneous flow visualizations.

Time resolved measurements in the outflow of a transonic compressor rotor operating near the compressor's peak efficiency points revealed high frequency (3 to 4 times blade passing) total pressure and temperature fluctuations of substantial amplitude in the core flow between the wakes, as well as large fluctuations in the wake strength of any particular blade [5], Fig. 1. Similar observations were made in three different single stage transonic compressors in three different test facilities using a variety of

high frequency response probe types [11]. The machines differed in design intent (both commercial fan and high speed military designs were included), but all operated at high rotor efficiency (above 90%). The outflow of all three rotors demonstrated similar types and degrees of rotor relative unsteadiness, the unsteadiness being maximum near the design or maximum efficiency operating point. This indicates that rotor relative unsteadiness is a common phenomenon in transonic compressors.

A laser anemometer physically measures one or more components of the instantaneous velocity at a point in space. Because of the relatively high level of turbulence common to turbomachinery flowfields, the instantaneous velocity measurements are usually averaged and the result presented as the average velocity at that point (Fig. 2a). The velocity statistics at the point can also be examined however (although this is not commonly done), and can be presented in terms of a probability density distribution (PDD), a histogram showing the number of observations made at each value of velocity. For a turbulent flow, the shape of this histogram should be Gaussian. Laser anemometer measurements in the vicinity of the passage shock have shown a bimodal velocity distribution indicative of a shock moving to either side of the measurement point [10]. These observations were explained in terms of small (0.5% of axial chord) motion of the passage shock about its mean position. Vortex shedding in the blade wake was advanced as a possible driver of this motion [5].

Subsequent laser anemometer measurements in the rotor wakes revealed that the velocity distributions were bimodal there as well; i.e., two velocities were equally likely with few measurements observed at the "average" velocity as it would be normally derived from such data [4], Fig. 2. Simultaneous time resolved temperature and pressure probe measurements in the rotor outflow

showed unsteadiness relative to the rotor at two time scales. One was the high frequency disturbances mentioned above. The second appeared primarily as a modulation of the wake flow with frequency components on the order of 1/2 to 3 times shaft rotational speed. This modulation could not be explained in terms of blade to blade geometric differences since the fluctuations were primarily aperiodic with rotor rotation (and thus not locked to the geometry) and were several times the magnitude of the periodic disturbances. A striking feature of the disturbances themselves was the large total temperature fluctuations in the wakes--±3-5% of the mean total temperature (i.e., 10-20°C)--indicating local regions of intense cooling and heating. The instantaneous adiabatic efficiency calculated from these measurements showed a concomitant variation with some local regions appearing as over 100%. These temporal fluctuations and laser anemometer measurements were explained as resulting from a vortex street structure in the blade wakes. The over 100% efficiency observations have yet to be explained.

3. DESCRIPTIONS OF THE BLADE WAKE AND VORTEX STREET

In the previous work, the wake was modelled as two staggered rectilinear rows of Rankine vortices of opposite sign in a uniform freestream [11]. The vortices consist of an inner region with a forced-vortex core and an outer region following the irrotational flowfield of a classic von Karman vortex street. This model was fit to the laser anemometer data so that the time averaged velocity profile and the statistical distribution of velocities (the probability density distribution) in the wake would match. The vortex size and strength were adjusted to fit the velocity profile while the ratio of the streamwise vortex spacing (A) to the distance between vortex rows (H) determined the velocity statistics (see Fig. 5).

As can be seen in Fig. 3, the model fits the data relatively well, which

is a consistency check. The model prediction of a shedding frequency of 16±2 kHz is quite close to the 14-15 kHz inferred from the core flow pressure fluctuations. Furthermore, the model readily explains the high level of fluctuations observed in the wake with the high frequency response probes. This is an artifact of sampling caused by the random position of the vortices in the wakes as the compressor revolves past the probe location. Figure 4 compares the absolute frame rotor outflow total pressure fluctuations predicted by the model with measurements.

While the vortex street model in [11] does a good job of explaining many of the experimental observations, it is a static model, describing the wake state only at a particular axial station. Thus, it contains no information on the vortex formation process, its evolution or decay. At this time we know of no published analytical model describing this process in detail.

4. DYNAMIC ENERGY REDISTRIBUTION

One of the more interesting implications of identifying the structure of the wake of a transonic compressor blade as containing a vortex street is that the unsteady pressure field in the blade relative frame can redistribute thermal energy. The vortex street propagates at a velocity different from that of the mean flow and entrains fluid into and through the wake. As the entrained fluid passes through the pressure field of the vortex, its total enthalpy can be changed. In essence, the vortex street can be thought of as an array of tiny turbomachines!

The dynamics of this problem have been addressed by McCune [12] with a straightforward unsteady energy equation analysis. He shows that the pressure field fluctuations from the vortices change the total temperature distribution in the fluid and that the amplitude of this effect scales with the square of the freestream Mach number. At Mach 1, the vortices are predicted to produce

a temperature fluctuation of 3-5% of the freestream total temperature, quite close to the observed value. This scaling with Mach number explains why the phenomenon was first noticed in a high speed machine (tip relative Mach number of 2.2).

Kurosaka et al. treat the problem in terms of the general Eckert-Weise effect [13] in which the recovery factor at the rear of a shedding right circular cylinder can be negative and the wake centerline cooled to below the freestream inflow value, showing that this is the result of vortex street behavior [14]. A key point is that this cooling by the vortices is observed with steady state instrumentation, i.e., the average centerline temperature is depressed. There must, of course, be a concomitant increase in total temperature in the surrounding flow outside the wake. Kurosaka also demonstrated that the vortex shedding and temperature separation can be significantly enhanced with acoustic feedback, essentially extending acoustic resonance work to include energy separation [6], [7].

The intense, localized hot and cold spots generated by the vortex street explain the large, abrupt temperature fluctuations observed in the time resolved total temperature measurements of the compressor wakes.

5. WAKE STRUCTURE EFFECTS ON APPARENT COMPRESSOR EFFICIENCY

An earlier work on high frequency passage shock motion driven by vortex shedding identified three mechanisms by which the loss in the compressor could increase [5]. The first is the increase in entropy rise across a shock wave undergoing small periodic axial motion compared to that for a steady shock at the same average approach Mach number. This change was quite small, amounting to only a 0.1 to 0.2 percent decrease of adiabatic efficiency in the rotor studied. The second loss source was the small scale nonuniformities in total pressure generated by the oscillating shock wave. In this case, it was

assumed that due to the small spatial extent of the perturbation (1/8~1/4 chord), the enthalpy would not be recovered as pressure rise in the diffusion process in the stator but rather appear as a mixing loss downstream. This loss was calculated to be of the same order as the wake mixing loss, about 1% (10% of the total measured stage loss). The third loss mechanism is the amplification of the spatial nonuniformities in the stage outflow, discussed above, by the shock system in a following transonic stage. This loss was estimated to be 2 to 3 times as great as that in the first stage, i.e., 2 to 3 percent of stage adiabatic efficiency.

In this section we wish to discuss not additional thermodynamic loss mechanisms (i.e., production of entropy), but rather apparent losses, artifacts induced in the measurement processes and their interpretation by the periodic nature of the wake structure. If not properly accounted for, these artifacts can result in an erroneous estimate of compressor performance.

Before doing so, however, we wish to point out a simple curiosity. Adiabatic efficiency is often used to express turbomachine loss (entropy production). In an unsteady, transonic flow, however, the change in adiabatic efficiency need not be congruent with the entropy production, as it must in a steady flow.

To illustrate this, we will define the local adiabatic efficency, η, in the usual manner relating the total pressure, P_t, and total temperature, T_t, ratios in the absolute (laboratory) frame as follows,

$$\eta = \frac{\left(\frac{P_{t2}}{P_{t1}}\right)_{abs}^{\frac{\gamma-1}{\gamma}} - 1}{\left(\frac{T_{t2}}{T_{t1}}\right)_{abs} - 1} \qquad (1)$$

where the subscripts 1 and 2 denote stations upstream and downstream of the

rotor blade. Station 1 is assumed to have uniform conditions of total temperature and pressure as would be the case with the first stage of a compressor. Station 2 consists of a freestream region and a wake region, with the blade wakes represented by vortex streets as modelled in [11]. The modelled wake total pressure and temperature contours are shown in Figs. 5 and 6. The change in entropy, S, from station 1 to station 2 may be expressed as,

$$e^{-(S_2-S_1)/c_p} = \frac{\left(\frac{P_{t2}}{P_{t1}}\right)_{abs}^{\frac{\gamma-1}{\gamma}}}{\left(\frac{T_{t2}}{T_{t1}}\right)_{abs}} \tag{2}$$

This can be seen in Fig. 7 for a flow with the compressor blade wake vortex model. The freestream stagnation temperature ratio is 1.175. As expected, the entropy variation is zero in the regions outside the vortex cores (since the model assumes that all the entropy change in the wakes is in the vortex cores themselves).

Equation (1) for the efficiency may now be re-written by eliminating the stagnation pressure ratio using Eq. (2).

$$\eta = \frac{\left(\frac{T_{t2}}{T_{t1}}\right)_{abs} e^{-(S_2-S_1)/c_p} - 1}{\left(\frac{T_{t2}}{T_{t1}}\right)_{abs} - 1} \tag{3}$$

Equation (3) shows that in a flow of uniform total temperature, the adiabatic efficiency is a unique function of the entropy change. Conversely, if there is no change in entropy from station 1 to station 2 then the efficiency is exactly 1.0 regardless of the variations in total temperature. However, if between stations 1 and 2 there is some loss mechanism (such as a normal shock wave) so that $S_2 > S_1$ in the freestream region, then the efficiency will be

less than 1.0 and, in fact, will vary through the flow as the total temperature varies. In the case of a transonic compressor with a vortex street wake, the efficiency will vary even outside the vortex cores in the wake (which contain all the entropy change) where the flow is otherwise modelled as irrotational and inviscid, i.e., the value of (S_2-S_1) is constant (as shown in Fig. 7). Since the flow in the absolute frame is unsteady (with or without vortex shedding) and the gradient of entropy is zero outside the cores, the total temperature must vary according to Crocco's theorem which may be written as follows,

$$T\vec{\nabla}S = \vec{\nabla}(c_p T_t) - \vec{q}(\nabla\times\vec{q}) + \frac{\partial\vec{q}}{\partial t} \tag{4}$$

In the regions outside the vortex cores this reduces to,

$$c_p\vec{\nabla}T_t = \frac{-\partial\vec{q}}{\partial t} \tag{5}$$

Equation (5) implies that the total pressure must vary as the total temperature changes so as to keep the entropy (S_2-S_1) constant. In any case, since (S_2-S_1) is constant and T_{t2}/T_{t1} varies throughout the vortex street, the efficiency will vary as well, even though the entropy is constant! This can be seen by comparing Figs. 7 and 8. The efficiency is not congruent with the entropy change. Because of the energy separation mechanisms discussed in Section 4, the total temperature in local regions can be greater or less than that of the freestream. Thus, there are regions in which the efficiency is greater than the freestream value. It should be pointed out with reference to Eq. (3) that, so long as the entropy increases, a variation in total temperature cannot result in an adiabatic efficiency above one.

It is important to note that this difference between entropy rise and efficiency requires only that the flow have a change in entropy between the measurement stations (e.g., a shock wave) and a spatial variation in total temperature. Unsteadiness plays a part only in that, in the absence of heat

conduction and viscous stresses [15], a variation in total temperature can only be produced by unsteady pressure forces. The unsteadiness is required in the absolute frame, not the blade relative frame, and thus a blade relative unsteady wake is not a prerequisite. Rather, this effect is common to all transonic and supersonic turbomachines. Other than suggesting that adiabatic efficiency is a misleading measure of turbomachine performance, the practical significance of this observation has yet to be enunciated, but the authors find it interesting.

The structure of the compressor blade wakes can make a difference in the aerodynamic efficiency as commonly measured with aerodynamic probes in the rotor outflow. To illustrate this, we will consider two transonic compressor rotors with the same geometry, true mass averaged total pressure and temperature rise, and, therefore, the same mixed out adiabatic efficiency. One blade will be assumed to have a classic turbulent wake while the other's wake will consist of a vortex street with the same average velocity defect. (Here we use the term turbulent rather loosely, meaning random, thus ignoring any turbulent structure which may exist.) In other words, the wakes as measured by conventional laser anemometry techniques would appear identical. Convertional, low frequency response probes are then used to accurately measure the true time average of the total temperature and pressure at the rotor outflow. (Since this is a two-dimensional analysis, the area averaged quantities measured by probes are actually line averages.) The probes are assumed to be free from dynamic effects. We will take the average flow conditions at the rotor blade row exit plane to be those measured in a transonic rotor [4], Table 1. Note that the total temperature is higher in the flow outside the wakes in the vortex street case compared to that in the turbulent wake case. This is required since the vortex street depresses the wake centerline temperature but the total energy flux out of the blade row must be the same in both cases.

TABLE 1
ROTOR EXIT CONDITIONS ASSUMED FOR MIXING CALCULATION

Freestream	Vortex Wake	Turbulent Wake
Total pressure ratio	1.646	1.646
Total temperature ratio	1.175	1.170
Absolute exit flow angle	45°	45°
Wake width/Passage width	0.260	0.260

Table 2 shows the resultant average flow condition calculated with the two wake states. Results are given both close to the rotor (the measurements were made at 130% of the axial chord) where the wake structures are distinct, and far downstream where the wakes have totally mixed out. The mass averaged quantities agree at both stations of course. The time averages close to the rotor do not, however. The time average of the vortex street wake case is quite close to the mass average (probably by coincidence) but the turbulent wake case efficiency is measured at over 1% low. (The difference between time or area and mass averages is well known. The point is that the low frequency response probes can only measure the time average.) Far downstream, the mass averaged efficiency has decreased by 1/2% (which is why probe stations are normally placed as far downstream as possible).

TABLE 2
ROTOR OUTFLOW AVERAGE LABORATORY FRAME CONDITIONS

	Vortex Wake	Turbulent Wake
Near Rotor (130% Axial Chord)		
Mass averaged total pressure ratio	1.644	1.642
Mass averaged total temperature ratio	1.175	1.175
Mass averaged adiabatic efficiency	0.873	0.871
Probe indicated total pressure ratio	1.644	1.641
Probe indicated total temperature ratio	1.175	1.177
Probe indicated adiabatic efficiency	0.872	0.859
Far Downstream (Mixed Out)		
Total pressure ratio	1.648	1.645
Total temperature ratio	1.177	1.176
Adiabatic efficiency	0.866	0.867

If the wake structure were always the same, the difference in measured efficiencies due to the structure could be mixed in with empirical probe calibration factors and thus be calibrated out (in theory). If, however, a small change in blade design or turbomachine operating point were to alter the wake structure alone, there would be an erroneous change in measured aerodynamic efficiency, an error of over 1% for the stage studied here. In other words, a change in the wake structure can appear as a change in stage efficiency, even though the momentum and thermal energy flux through the machine (the pressure and temperature rise) have not changed. This error would disappear if the measurements were made with sufficient time resolution to resolve the wake structure.

Thus, wake structure can introduce artifacts in the measurement of compressor performance, introducing apparent changes not representative of the state of the fluid exiting the machine. Because the magnitude of the temperature separation in the vortex street scales with the square of the Mach number, this effect should be most important for transonic and supersonic turbomachines. The argument should hold true for turbine flows as well, but this has not been verified.

6. NUMERICAL SIMULATION OF COMPRESSOR BLADE WAKE SHEDDING

To further investigate the compressor wake structure, the flow through a single blade passage was simulated with a computational fluid dynamic (CFD) technique. A two-dimensional, time accurate, Reynolds averaged, explicit Navier-Stokes calculation was done with a relatively fine grid and very small time step to insure good spatial and temporal resolution. The midspan airfoil geometry of the transonic rotor measured in [4] was used. To accomodate supersonic inflow limitations in the code, the inlet relative Mach number was reduced from the 1.17 of the measurement condition to 0.92 for the calculation.

Inlet total conditions were adjusted to keep the Reynolds number based on axial chord at 1.2×10^6. The inlet flow at the upstream boundary is specified as uniform. Thus, there is no external excitation or periodicity, only that generated by the flow itself. More details on the calculation can be found in [15].

The primary observation to be made from this ab initio calculation is that vortices are shed into the blade wake. Figure 9 is a plot of instantaneous velocity vectors in the blade relative frame near the trailing edge. It shows the vortex structure in the wake as well as a separated region on the suction surface. (The vector length denotes the magnitude of the local flow velocity, the orientation the flow direction.) Only two vortices are readily seen here due to the change in vortex core translational velocity as the vortices propagate downstream. This has the effect of blurring the flow structure in any frame other than that moving with the cores. A similar problem in visualizing the vortices was encountered in the modelling effort [11]. In both cases, the ready identification of the vortex structure is strongly dependent on the frame of reference chosen, making the vortex street fairly elusive and hard to see.

The shedding periodicity shows up quite clearly in the calculated trailing edge static pressure, Fig. 10. Also of interest is the lower frequency present which modulates both the amplitude and the frequency of the vortex shedding. This is quite similar to low frequency modulation observed in the experimental measurements [11]. In the simulation, the lower frequency correlates with the motion of the separation point along the suction surface and with axial motion of the passage shock, and thus may be a shock boundary layer interaction, Fig. 11. There is also a 30% fluctuation in blade moment at this frequency, which is low enough ($\sim$350 Hz) to be of concern to the

structural designer. The exact cause of this low frequency movement of the separation point is not yet clear but appears quite similar to instabilities observed in high speed diffusers.

The modulation of the vortex shedding frequency by the low frequency oscillation was considerable, a factor of two. The strength of the vortices varied inversely with the shedding frequency. The shedding frequency range from the CFD calculation is compared with those inferred from the laser anemometer probability density distributions and from the core flow-shock motion fluctuations in Fig. 12. These three estimates are completely independent and show quite good agreement. The large fluctuations in frequency shown in the numerical simulation tend to explain the difficulty encountered in extracting a single, unambiguous frequency estimate from the experimental measurements. Fluctuations of this magnitude may also blur the bimodal anemometer histograms.

The blade relative total pressure in the numerical simulation as would be measured with a fixed laboratory frame probe as the rotor passes is compared with measurements [11] in Fig. 13. The qualitative agreement is excellent. The calculation clearly captures the wake modulation evident in the measurements.

The high frequency jitter of the passage shock at the shedding frequency inferred in [5] is not observed in the calculation. However, since the predicted shock motion is no more than one grid cell size and the numerics spread the shock over five grid points, this is not surprising. A calculation with a much finer grid size would be required in order to address this problem properly.

Overall, the numerical, CFD simulation agrees extremely well with the experimental observations and the analytical model. The one area in which the numerical simulation does not add information is the decay of the wake

structure as it is convected downstream since the numerical damping overwhelms most physical dissipation mechanisms.

7. DISCUSSION AND CONCLUSIONS

Considerable effort has traditionally been spent on establishing the proper parameter with which to correlate vortex shedding. A Strouhal number based on trailing edge thickness is commonly used, especially for blunt trailing edge bodies [2], [3], [9]. For compressor blades, the wake displacement thickness has been suggested as a more realistic correlation [5]. Since the wakes of compressor blades are relatively thick compared to the trailing edge, the difference between the correlations using the different parameters is considerable, a factor of four in frequency. For the blade section studied here, a frequency of 15 kHz is predicted using the wake thickness, matching both the experimental and numerical results.

The modulation of the frequency and strength of the vortex shedding observed in the CFD calculation is extremely important for the interpretation of experimental measurements. The presence of the modulation considerably complicates the practical problem of vortex detection in rotating machinery. The impact on laser anemometry techniques and spectral analysis methods needs to be quantitatively assessed.

Examination of the details of the numerical simulation as well as classical vortex shedding analysis [16] suggests that the process may be considerably more complex than can be represented by a simple Strouhal number. Many shedding processes may compete and the separation zone observed in the simulation certainly plays a part. A more complete discussion of vortex formation and evolution will be the subject of a later paper.

This work has tended to treat the compressor blade and vortex street in isolation when in reality it is part of a very complex environment. Acoustic

feedback has been shown to both enhance shedding and alter the frequency [7], [13], [19]. There are many mechanisms involving inter-blade row interactions for forcing the shedding as well. The possibility of phase locking between blades is also evident [17]. Clearly much work can be done in this area.

Laser anemometer measurements of the turbulent kinetic energy within the stator passages of a transonic compressor stage have shown a structure consistent with a vortex street wake (i.e., periodic islands of high kinetic energy in the wake) [18]. A laser anemometer measures the stationary frame ensemble averaged flowfield. Thus, the vortices must be shed at fixed phase relative to the stator in order to appear in the data. This implies that there is an additional mechanism by which the measurement of time averaged performance using closely coupled instrumentation (in the stator leading edge, for example) may give misleading results. The assumption that the flowfield is well sampled would no longer be valid. The stage geometry is such that a stationary frame probe would sample along a vertical line in the flow maps given in Figs. 6-8. Phase locking implies that the patterns evident in the figures are stationary in the flow-wise direction with respect to the measurement station. Thus, the probe will not be uniformly surveying the flowfield. The quantitative importance of this effect has yet to be determined.

Another area needing more investigation is the three-dimensional wake structure in real turbomachines. Although it is often dangerous to generalize from two to three dimensions, we will point out that if the vortices have considerable spanwise extent, they can serve as an extremely powerful mechanism for the radial transport of fluid--complicating the evaluation of the radial work and efficiency distributions. Work with cylinder shedding has shown that external forcing (acoustic in this case) can enhance the spanwise coherence of the shed vortex street [19].

A change in measured performance due to the wake structure is a result of the difference between common probe (generally time) averages and true mass averages. Thus, in addition to the vortex wake structure discussed in this paper, other processes which redistribute thermal energy in the flow (and thus change the difference between the averages) can have similar effects. Local heat transfer, either within the flow or to the blades, may be important in this regard. Furthermore, the dynamic behavior of aerodynamic probes can introduce artifacts into the performance measurements which could either amplify or reduce the effects noted above, depending upon the exact structure of the flow.

In this paper we have made the following observations concerning the structure of compressor blade flow and wakes:

1. The wakes of high Reynolds number, transonic compressor blades can consist of shed vortex streets. This is confirmed by measurement, modelling, and numerical simulation.
2. The vortex shedding scales with wake thickness.
3. The shedding frequency and strength are sensitive to the environment.
4. The vortex street can depress the average wake temperature.
5. The importance of the wake structure increases with the square of the freestream Mach number.
6. Wake structure can influence the measurement of compressor efficiency.
7. Changes in wake structure can be mistaken for changes in compressor performance.
8. The wake structure can drive the blade shock system, inducing loss.
9. The wake structure can be influenced by other fluid dynamic instabilities present in a blade passage which themselves may be important for performance and structural dynamic reasons.

10. Caution is required when interpreting steady state solutions of inherently unsteady flowfields.

Overall, vortex shedding in transonic compressor blade wakes can have significant influence on compressor behavior.

8. ACKNOWLEDGEMENTS

The authors would like to thank Mr. R. Haimes for assistance with the numerical simulation (he wrote the code), and E.M. Greitzer for many useful discussions. This work was supported in part by the U.S. Air Force Office of Scientific Research and the NASA Lewis Research Center.

9. REFERENCES

1. Davies, M.R.D. and Bryanston-Cross, P.J., "Holographic Measurements and Theoretical Predictions of Unsteady Flow in a Transonic Annular Cascade," J. Eng. for Power, Vol. 107, No. 2, 1985.

2. Heinemann, H.J. and Butefisch, K.A., "Determination of the Vortex Shedding Frequency of Cascades with Different Trailing Edge Thicknesses," AGARD CP-227, 1977, pp. 35-1 to 35-10.

3. Heinemann, H.J., Lawaczeck, O., Butefisch, K.A., "V. Karman Vortices and Their Frequency Determination in the Wakes of Profiles in the Sub- and Transonic Regimes," IUTAM Symposium, 1976, pp. 75-82.

4. Hathaway, M.D., Gertz, J.B., Epstein, A.H. and Strazisar, A.J., "Rotor Wake Characteristics of a Transonic Axial Flow Fan," AIAA Paper 85-1133, July 1985.

5. Ng, W.G. and Epstein, A.H., "Unsteady Losses in Transonic Compressors," J. Eng. for Power, Vol. 107, No. 2, 1985.

6. Cumpsty, N.A. and Whitehead, D.S., "The Excitation of Acoustic Resonances By Vortex Shedding," J. Sound Vib., Vol. 18, No. 3, 1971.

7. Parker, R., "An Investigation of Acoustic Resonance Effects in an Axial Flow Compressor Stage," J. Sound Vib., Vol. 8, No. 2, 1968.

8. Hobbs, D.E., et al., "Experimental Investigation of Compressor Cascade Wakes," ASME 82-GT-299, April 1982.

9. Blake, W.K., "Excitation of Plates and Hydrofoils by Trailing Edge Flows," J. of Vib., Acoustics, Stress, & Rel. in Des., Vol. 106, July 1984.

10. Strazisar, A.J., "Investigation of Flow Phenomena in a Transonic Fan Rotor Using a Laser Anemometer," J. of Eng. Power, Vol. 107, No. 2, April 1985.

11. Gertz, J.B., "Unsteady Design Point Flow Phenomena in Transonic Compressors," MIT Ph.D. Thesis, September 1985.

12. McCune, J.E., "Theoretical Modelling of Stability and Unsteadiness in Transonic Compressor Flow Fields," Annual Technical Report to AFOSR, "Fluid Dynamics of High Performance Turbomachines," MIT GTL, November 1985.

13. Eckert, E.R.G., "Energy Separation in Fluid Streams," Int. Comm. Heat Mass Transfer, Vol. 13, 1986, pp. 127-143.

14. Kurosaka, M., Gertz, J., Graham, Goodman, J.R., Sundaram, Riner, W.C. and Kuroda, H., "Energy Separation in a Vortex Street," in publication, J. Fluid Mech., 1986.

15. Owen, P.R., "Computational Simulation of Unsteady Flow in a Transonic Compressor Rotor," MIT S.M. Thesis, September 1986.

16. Morkovin, M.V., "Flow Around Circular Cylinder - A Kaleidoscope of Challenging Fluid Phenomena," in Symposium on Fully Separated Flows, A.G. Hansen, Ed., ASME, New York, 1964.

17. Camus, J.J. and Bryanston-Cross, P.J., "1 MHz Bandwidth, Real Time Schlieren Techniques in a Linear Cascade," Proc. of Symposium Measurement Techniques in Transonic and Supersonic Flows in Cascades and Turbomachines, Lyon, 1981.

18. Dunker, R.J., "Flow Measurements in the Stator Row of a Single Stage Transonic Axial Compressor With Controlled Diffusion Stator Blades," AGARD CP-351, 1983.

19. Blevins, R.D., "The Effect of Sound on Vortex Shedding From Cylinders," J. Fluid Mech., Vol. 161, 1985, pp. 217-237.

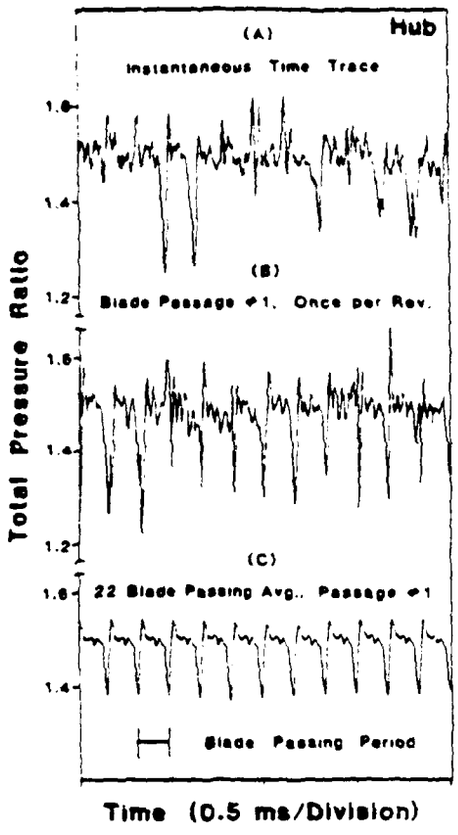

Fig. 1: Transonic compressor rotor exit total pressure near hub: (A) instantaneous measurement, (B) an individual blade passage as seen once per revolution, and (C) an ensemble average of that individual passage, from [5]

Fig. 2: Laser anemometer measurement of the outflow from a transonic compressor rotor: (A) average velocity profile, (B) histogram of velocity statistics in core flow showing Gaussian profile characteristic of turbulence, and (C) velocity statistics in wake showing bimodal distribution attributed to vortex street, from [4] (below)

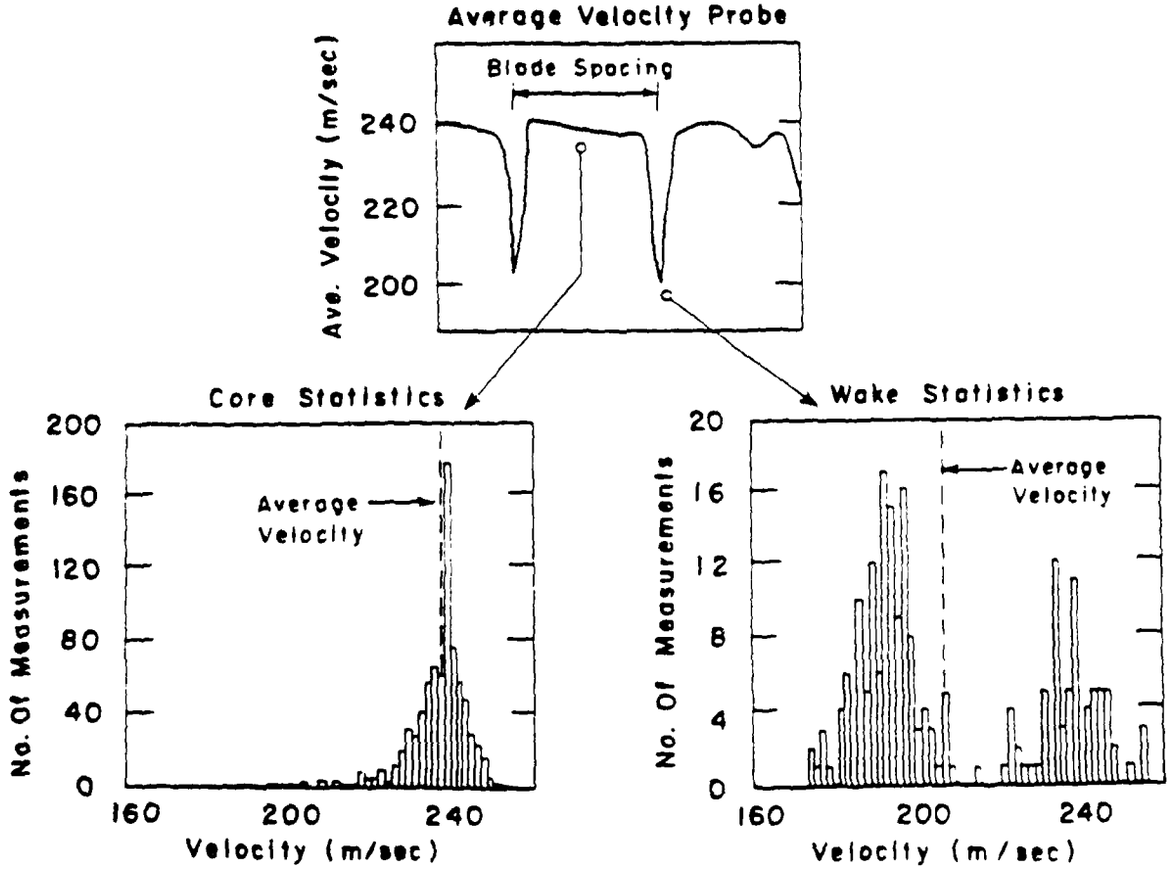

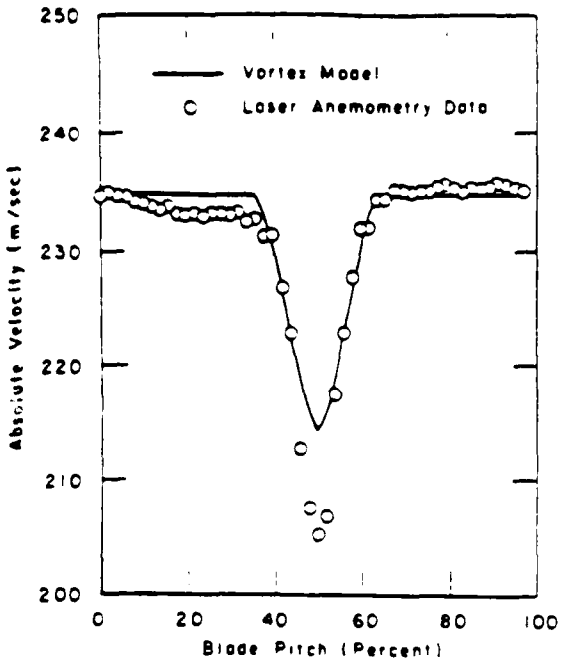

Fig. 3: Comparison of mean absolute velocity measured by a laser anemometer in a rotor blade passage with that from the average of the vortex street model [4]

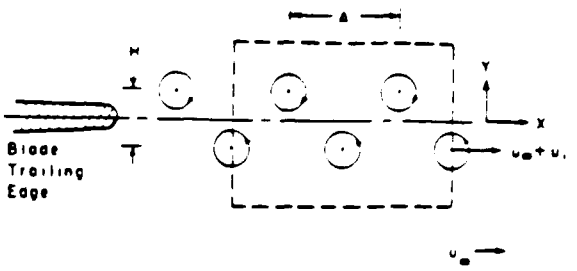

Fig. 5: A schematic representation of the vortex street geometry used in the model. The box delineates the region illustrated in Figs. 6, 7 and 8.

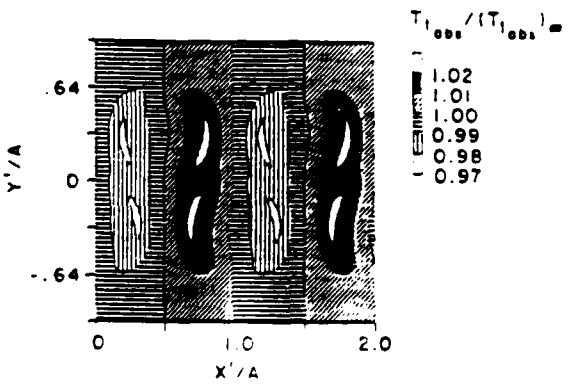

Fig. 6a: A contour plot of absolute total temperature contours predicted by wake model

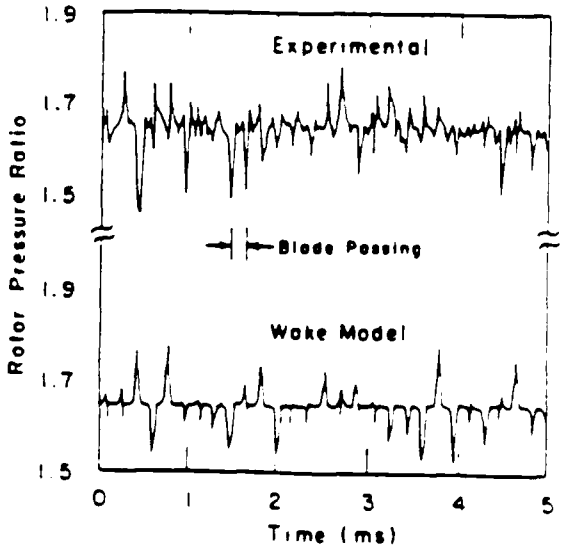

Fig. 4: A comparison of the time resolved rotor exit absolute total pressure with that predicted by the vortex street model, from [11]

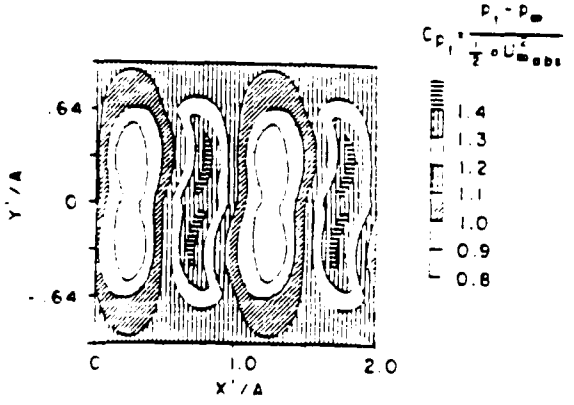

Fig. 6b: A contour plot of absolute total pressure contours predicted by wake model

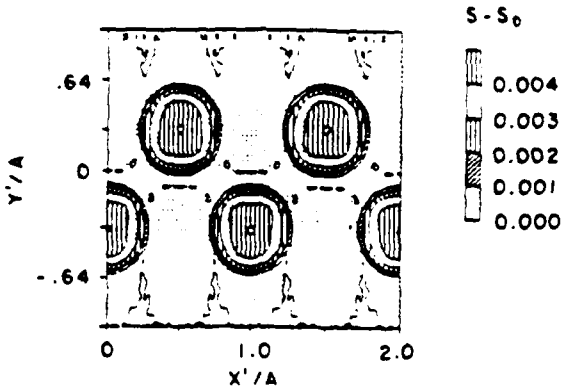

Fig. 7: Contours of entropy rise from wake model. Note that the entropy is essentially constant outside the vortex cores

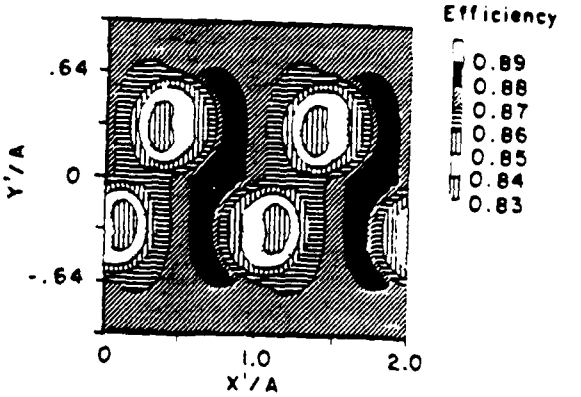

Fig. 8: Contours of adiabatic efficiency from the wake model. Note that these regions are not congruent with the entropy change in Fig. 7 and that there are regions of adiabatic efficiency indicated as above that of the freestream.

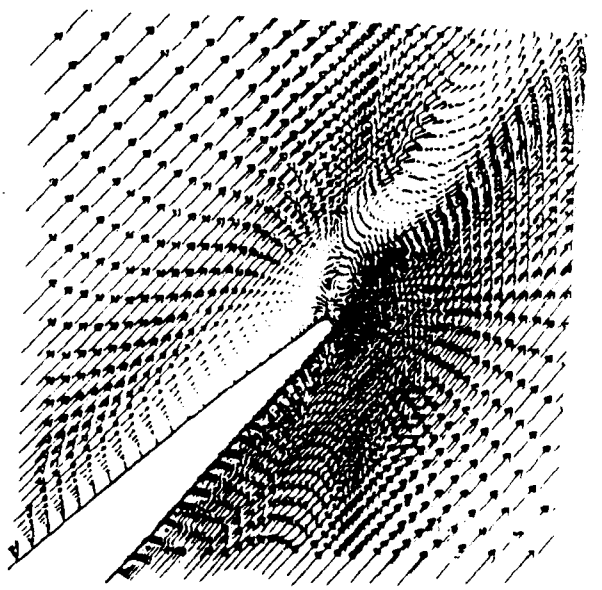

Fig. 9: Instantaneous vector plot (arrow orientation is velocity direction, length is velocity magnitude) of the trailing edge region of a transonic airfoil calculated with a 2-D time accurate Navier-Stokes code. Note the separated region on the suction surface and the vortices shed into the wake.

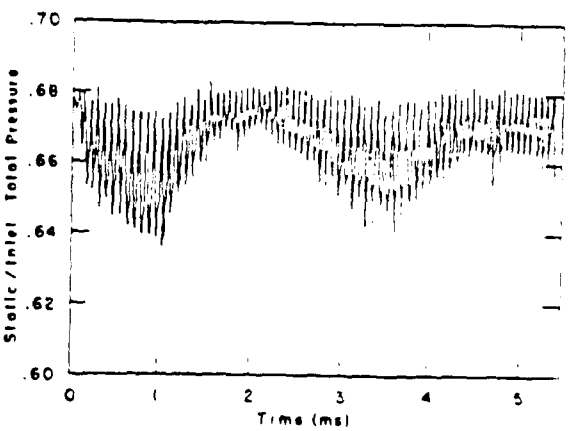

Fig. 10: Static pressure history at trailing edge of a transonic airfoil. Note the periodicity due to vortex shedding and the modulation of that shedding by a lower frequency disturbance.

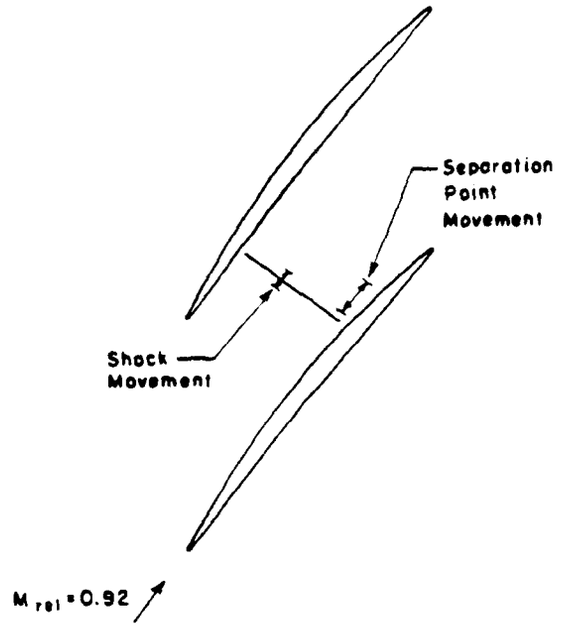

Fig. 11: The numerical simulation shows a correlation between the passage shock motion and the separation point movement

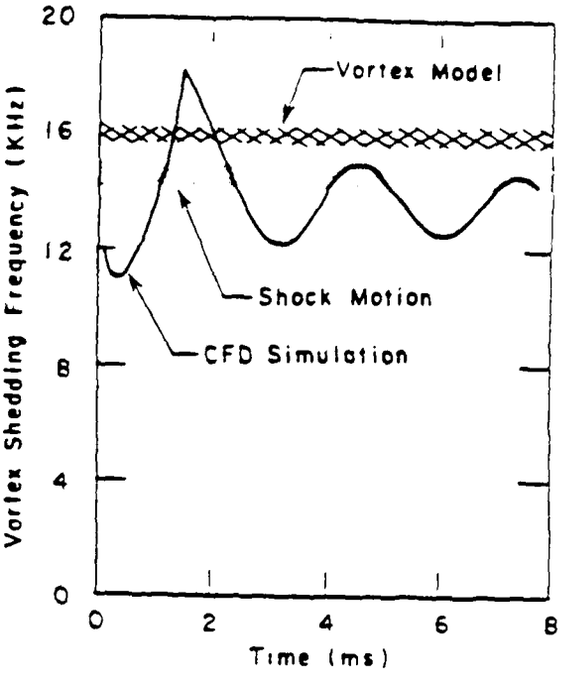

Fig. 12: A comparison of the shedding frequency predicted by the CFD simulation with those inferred from measurements

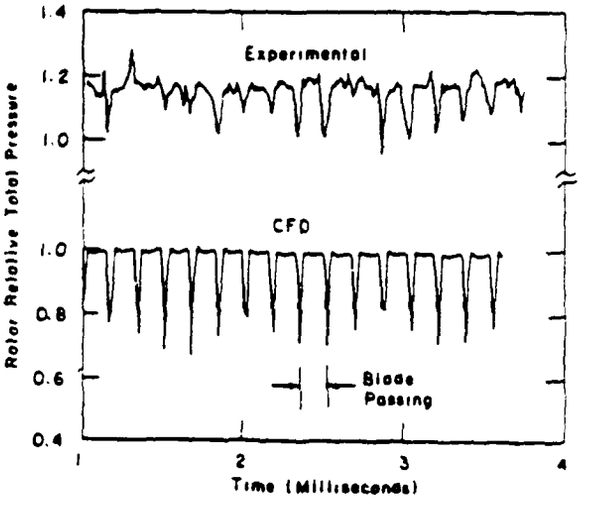

Fig. 13: A comparison of the rotor relative total pressure time history measured in a transonic compressor with that predicted by the CFD simulation

TASK II: EXPERIMENTAL AND THEORETICAL STUDY OF FLOWS IN COMPRESSOR HUB/CASING TREATMENT

(Investigators: E.M. Greitzer, C.S. Tan, N. Lee)

APPROACH

This project is a combined analytical/experimental investigation of the flow phenomena responsible for the substantial enhancement of compressor stability found using casing/hub treatment. The work is focussed on detailed examination of differences in endwall flow features associated with an endwall configuration that has worked extremely well in improving stable flow range. A further issue, much wider in scope, is the general question of just what is "compressor stall" and what are fruitful approaches to delaying its onset.

To address this point, first-of-a-kind experiments with controlled hub slot suction and injection, and basic computations of the flow in the grooves have been carried out.

EXPERIMENTAL WORK

Background

During the past year, most of the effort has been spent on the experimental work. As described previously, an experimental facility was designed with a cantilevered stator row and a rotating hub. Blading parameters were chosen so that the stator (rather than the rotor) stalled first, stall occurred at the stator hub, the stall was wall stall, and the experiment was set up to simulate the flow over the tip of a rotor.

The detailed measurements taken with hub slots showed that the suction at the rear of the stator passage was very effective in suppressing the growth of blockage and hence rotating stall [1]. However, the use of a closed slot meant that there was no way to separate the presence of the suction from the presence of the jet out of the front of the grooves, and hence to conclusively identify which mechanism, suction from the rear or high velocity flow injection

from the front of the slot, was more important. For this reason, an experiment was set up to provide, separately, injection or suction. The experiments, which are described in the next section, used a slotted hub open to an inner plenum chamber, through which a controlled amount of suction or injection flow could be fed.

Overall Experiment Description

There are two parts to the present experiment. Part one is an examination of the effect of injection or removal flow rate on the pressure rise characteristics (speedlines). This has almost been completed. Part two will be focussed on the detailed stator flowfield measurement, also with injection/removal. This will take place after the completion of part one.

A total of four hubs were machined for the experiment. All were 60 degree axial skewed (Fig. 1), but the axial length of the slots and their location on the hub varied (see Fig. 2). The slots extended all the way through the hubs, i.e., were open to the plenum. The hubs originally machined are designated as:

Full 1 inch slot

1/4 inch open at rear (denoted as trailing edge in figure)

1/2 inch open at front (denoted as leading edge in figure)

1/2 inch open at rear

In addition, The full 1 inch slot was subsequently modified to yield another slot, open 1/4 inch at the front. The full 1 inch slot one had slots covering the middle 90% of the axial chord of the stator. The 1/4 inch open at rear had slots, 1/4 inch long axially, close to the stator trailing edge, etc.

The main features of this part of the experiment are summarized as follows:

- All speedlines were taken at a compressor speed of 2600 rpm, corresponding

to a rotor tip Mach number of 0.24 and a Reynolds number based on blade chord at the stator midspan of $1.0*10^5$. (Previous tests showed that there was little Reynolds number sensitivity for the baseline hub treatment configuration.)

- The smooth hub and the 1 inch treated hub were first tested without injection/removal. After that, a run was made using the 1" treated hub with the bottom of the slots sealed to eliminate interactions between the slots and the plenum.
- Different hubs were then tested with the injection/removal rate varied. The maximum rate was 7% of the main flow. With the 1/4 inch builds this led to too low a plenum pressure, and damage to the seal, so these builds were tested only up to suction rates of 3.5%. For reference, the measured mass flow (in and out) through the original hub treatment was approximately 3.5%.
- In the tests, the flow near the stator hub was monitored by hotwire; this proved helpful in identifying the stall point.
- Control experiments were carried out to verify that leakage through the seal had no effects on the speedlines.

Compressor Performance: Speedlines

Speedlines were taken for all of the hubs as described above and the dependence of stator static-to-static pressure rise on a) compressor flow rate, and b) injection/removal rate documented. In this report, static pressure rise (DP) is non-dimensionalized by $0.5\ \rho U^2$, where U is the mean rotor blade speed, unless otherwise stated. The compressor flow rate is presented as the flow coefficient, C_x/U, measured upstream of the inlet guide vanes. Injection/removal rate is shown as percentage of the compressor flow at $C_x/U = 0.35$.

The figure of merit used here to assess the degree of effectiveness of any treatment is the non-dimensional peak static pressure rise attained, $DP/0.5\rho U^2$. Although this can be debated with, the basis for use of this criterion is that it is the endwall regions which give rise to the stall, and what we are really assessing is the ability of the endwall regions to cope with a given pressure rise. (Note that relying on flow coefficient at the stall point is somewhat ambiguous because the flow coefficient was measured upstream of the stator. Had it been measured downstream, those speedlines with flow removal would have shifted to the left (that is, towards lower C_x/U) and those with flow injection to the right. Normalizing by $\frac{1}{2}\rho C^2$, where C is the inlet velocity, also carries some ambiguity because of this. For these reasons we have adopted the convention just described.)

Baseline Runs

The baseline runs, which are the smooth wall build and the 1 inch treated build (sealed), are discussed first. The smooth wall speedline is displayed in Fig. 3, together with the two cases tested with the 1 inch treated hub. The smooth wall plot is similar to that obtained previously, stalling at $C_x/U = 0.337$ and $DP/0.5\rho U^2 = 0.083$.

The same figure shows results from the 1 inch treated hub, sealed to decouple the flow in the slots from the plenum. For this case, stall occurred at $C_x/U = 0.303$, with peak $DP/0.5\rho U^2 = 0.137$.

With the 1 inch treated hub unsealed, the stall was delayed to an even lower C_x/U of 0.295, a 13% decrease in C_x/U compared to the smooth wall case. The peak $DP/0.5\rho U^2$ attained, as well as the abruptness of the drop at stall, was the same as before.

Speedlines: No Injection or Removal

Figure 4 presents the speedlines obtained with no fluid injection or

removal. Compared to the smooth wall build, the 1/4 inch hubs gave an improvement of 5%, whereas the 1/2 inch builds achieved 36% and 38%. The drop in performance of the 1/2 inch slots at stall was similar to that of the 1 inch slots.

Speedlines With Flow Removal

Figures 5, 6 and 7 show speedlines of the 1/2 inch and 1/4 inch builds with different suction rates. The speedlines are arranged such that those for the same build are shown together in one of these three figures. The baselines are included for comparison.

Compared to the smooth wall characteristic, it appears that stall was suppressed regardless of where (front or rear) or how (1/2 inch or 1/4 inch) this suction was applied. The amount of increase in peak pressure rise was roughly the same for a given mass extraction independent of the slot geometry. With suction at the rear, however, performance generally dropped abruptly at stall. This was not so when suction was applied at the front.

Speedlines With Flow Injection

Speedlines obtained with different injection rates are shown in Figs. 8 through 10. Injection at the stator hub increased the stalling pressure rise, with injection at the front of the passage being more effective than injection at the rear. Injection at the rear resulted in a rather abrupt drop in performance at stall, whereas, with injection at the front, the effect of the stall onset on the compressor characteristic was very mild.

Effect of Slot Flow Rate on Peak Pressure Rise

In Fig. 11, stalling pressure rise is plotted with injection/removal rate for all of the hubs. The results are first of a kind which shows the effect of mass flow rate and injection/suction location on stall onset.

For the 1/4 inch slots, the stalling pressure rise increased monotonically

with suction rate in the whole suction domain. For the 1/2 inch slot tested, however, this was not the case. With no suction, the increase in stalling pressure rise of the latter was 38%. As suction increased from null, there was an initial drop in performance, reaching a lowest value at about 1.5% suction, after which it improved with no further drop. The zero-suction value was reattained at 2.2% suction.

All four slots had closely similar performance for suction higher than 2%, with the performance at the level of the 1 inch treated hub (sealed) at 4.5% suction.

Using $DP/0.5\rho U^2$ as a criterion with blowing, the slots at the front of the passage performed better than those at the rear at the same injection rate throughout the injection domain. For the 1/2 inch build, the "dip" in performance occurred in much the same way as with suction. Note that, even at 6% blowing rate, the stalling pressure rise was lower than that achieved by the 1 inch sealed treated hub.

Work During the Next Contract Period

Although there are some points to fill in on our study of the effect of injection and removal, this part of the experiment can be regarded as almost complete. The next major task is to take the detailed hot wire measurements in the stator passage to compare with the hub treatment measurements. This will be done over the next two months. In addition, we plan to spend considerable time in analysis of both the hot wire and the overall results.

It is to be emphasized that all of the results presented above are relatively recent, and we have not yet analyzed them in any sort of depth. Some preliminary conclusions, however, can be drawn. First, suction does appear to be slightly more effective than injection from the front part of the passage, and considerably more effective than injection in the rear part of the passage,

for flow rates up to that measured with the original hub treatment. For higher suction/injection flow rates, the suction appears to have a significantly stronger effect on peak pressure rise.

Second, although it is clear that the suction is quite important, as hypothesized, it is also clear that the actual situation is much more complex than can be explained by suction alone, and that with the treatment slots, the injection near the front end is also of use.

Beyond this, there are other issues which we have not yet addressed. Key among these is the basic question of what phenomena comprise compressor stall. In particular, the hot wire results from the previous experiments with the hub treatment showed that the fluid on the hub had a high dynamic pressure near the rear of the stator passage, but that the direction of the flow was basically tangential, with a very low axial velocity. Where did this fluid come from, and what determines the velocity field near the wall? Questions such as this are not at all resolved, but are at the heart of any type of rational analysis of stall and flow field instability.

Analytical Work

During the past year we have extended the simple analysis, reported on previously, for the flow in the grooves. The overall conclusions were similar to those reported before concerning the comparisons of computation and experimental measurements for mass flow into and out of the grooves, and hence will not be discussed in any detail. The main point is that the analysis is now on a more rigorous, less ad hoc, basis. The level of effort on this work has decreased with the departure of Dr. Modi, although a detailed report on the work is in preparation.

The next step in the analysis of the interaction of the flow in the grooves and that in the stator (or rotor) passage should, we think, make use

of the three-dimensional computational procedures that are now being developed. Two computations in particular suggest themself. First of all, a blade passage with a rotating endwall, such as is in the present experiment, as well as in rotor tips. Second, some modification to the calculation to try to simulate the inflow and outflow from the grooves, in order to see if the observed trends in peak pressure rise versus groove geometry can indeed be calculated. We hope to attempt this as a collaborative effort with Allison personnel.

Reference

1. Johnson, M.C. and Greitzer, E.M., "Effects of Slotted Hub and Casing Treatments on Compressor Endwall Flow Fields," to be published in ASME J. Eng. Gas Turbines and Power.

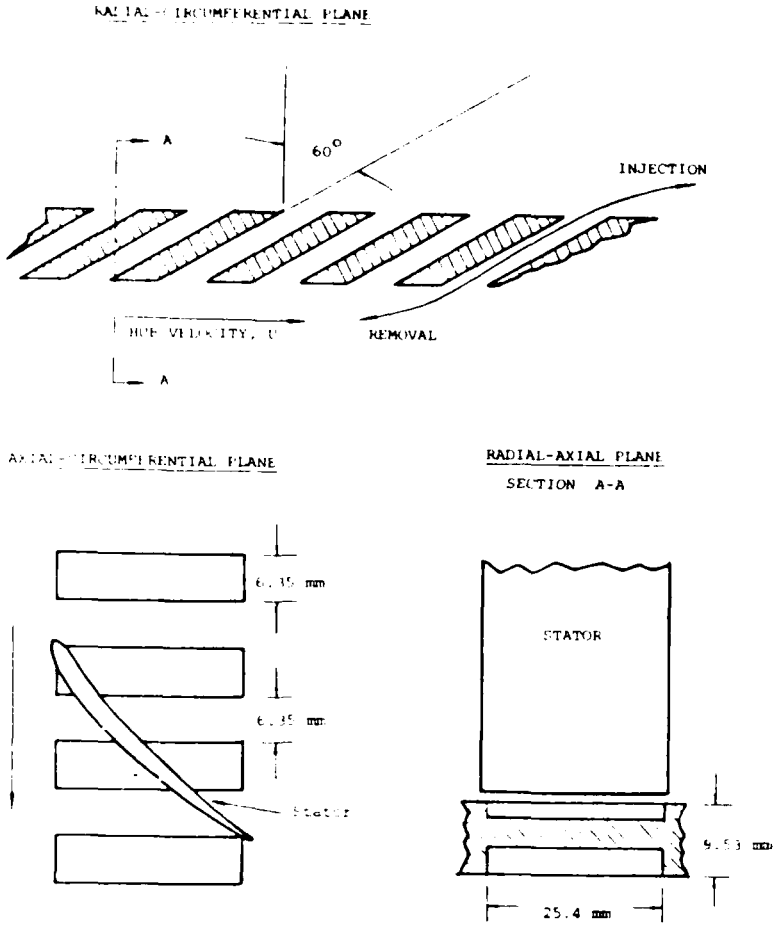

Fig 1 Geometry of 1-inch hub treatment

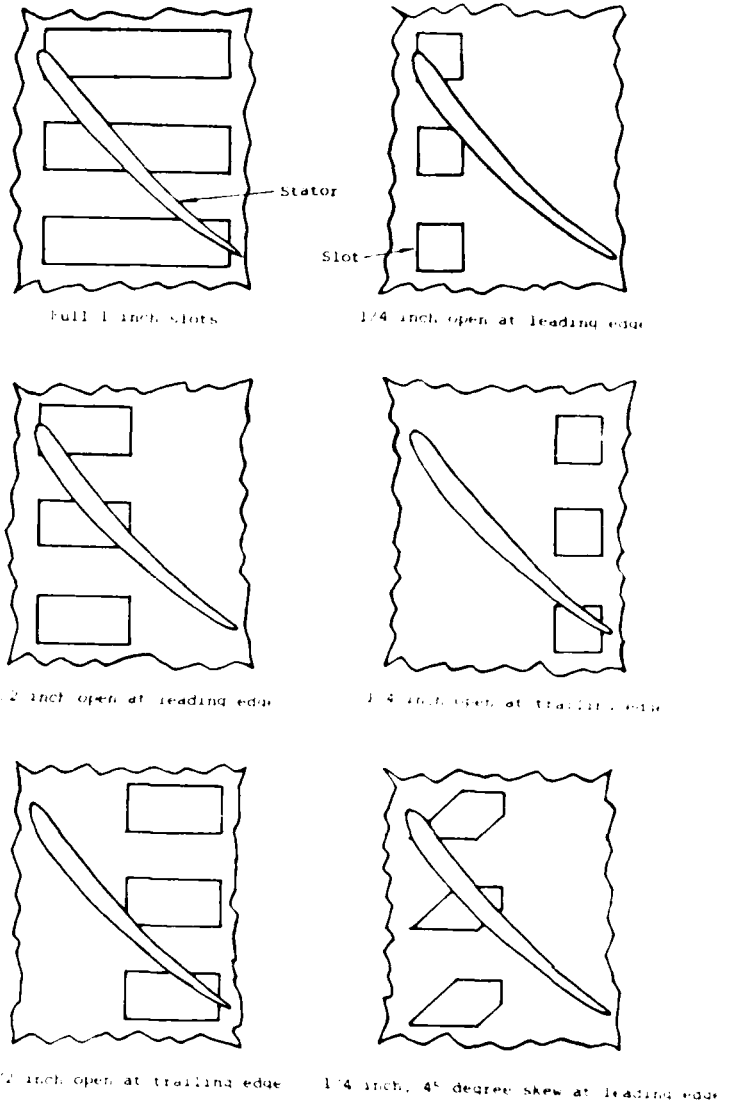

Fig 2 Slot locations of hub treatment

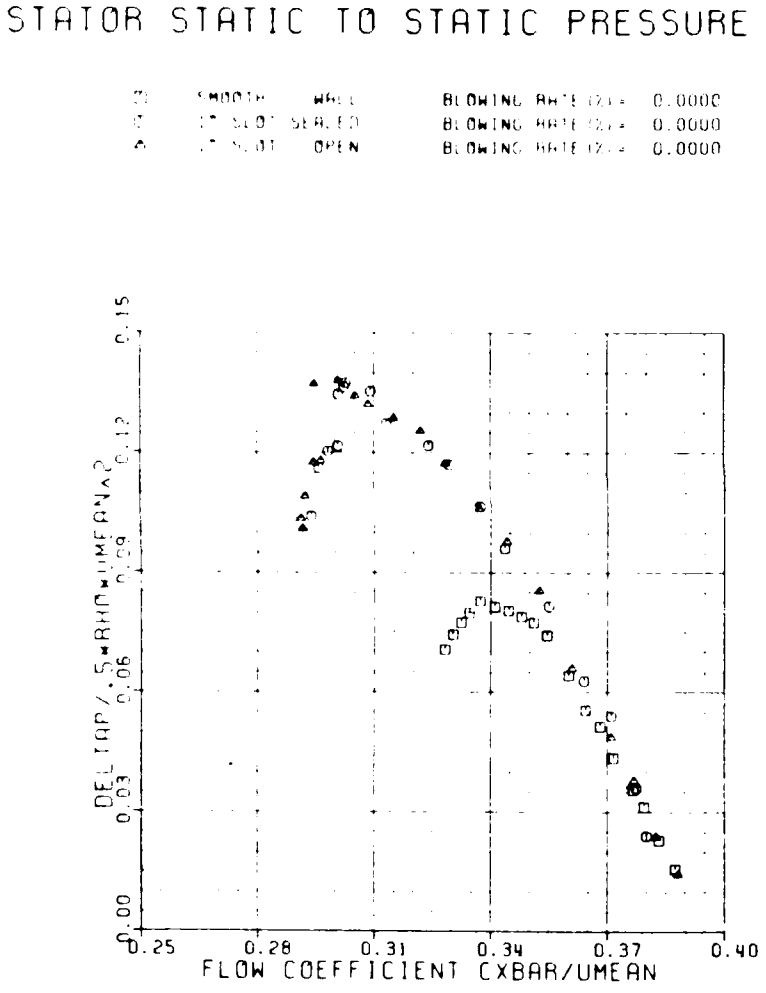

FIG 3 Baselines: Smooth wall and 1-inch hub treatment

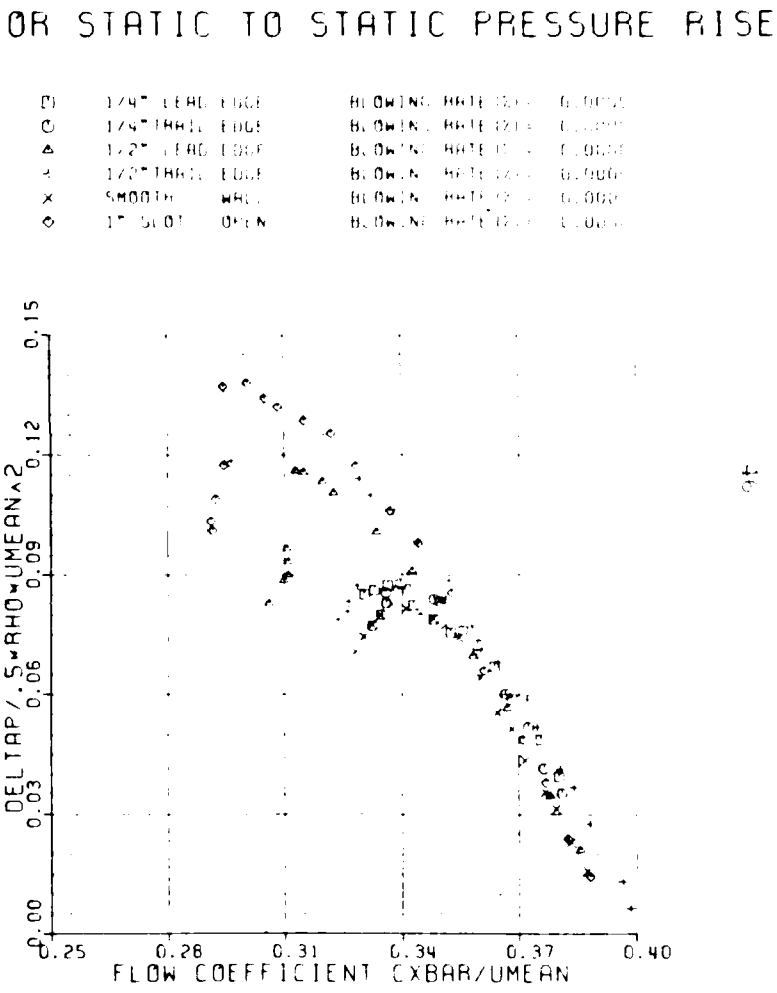

Fig 4 Speedlines: No injection or removal

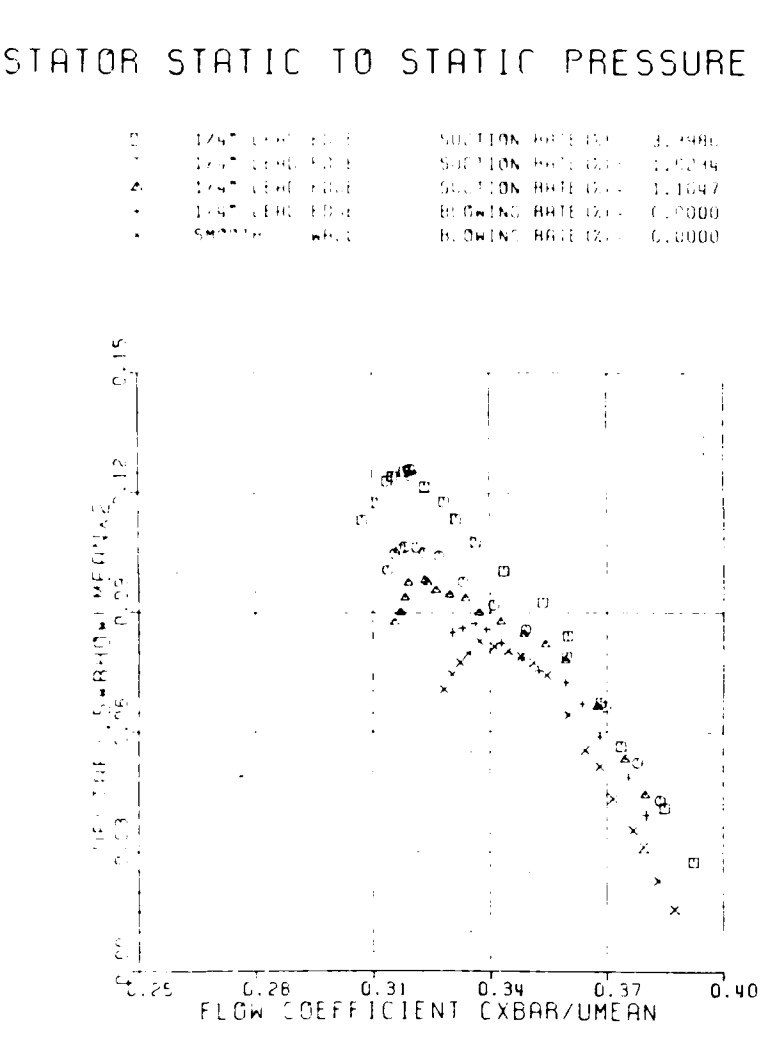

Fig 5 Speedlines: Suction over front quarter of stator

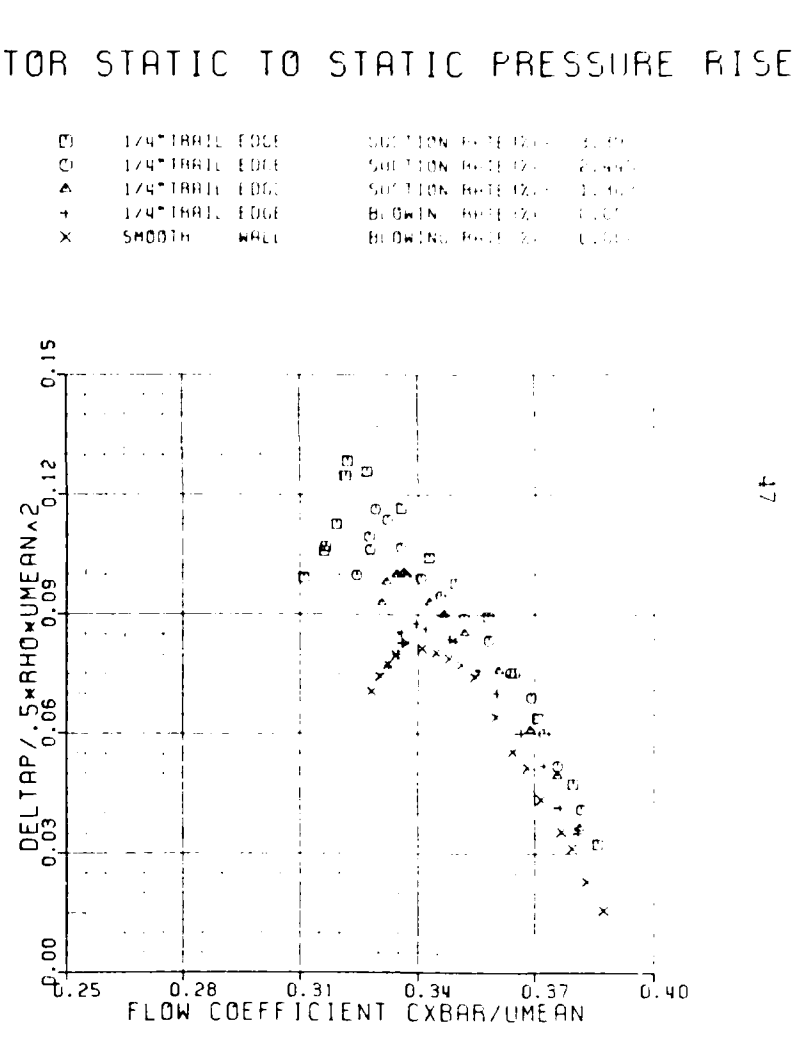

Fig 6 Speedlines: Suction over rear quarter of stator

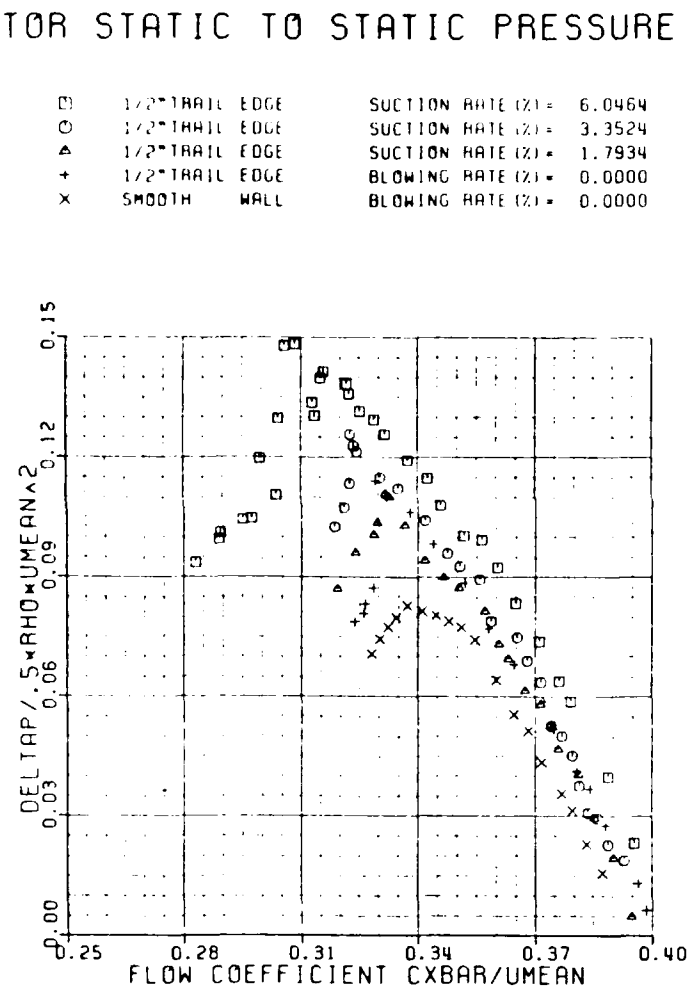

Fig 7 Speedlines: Suction over rear half of stator

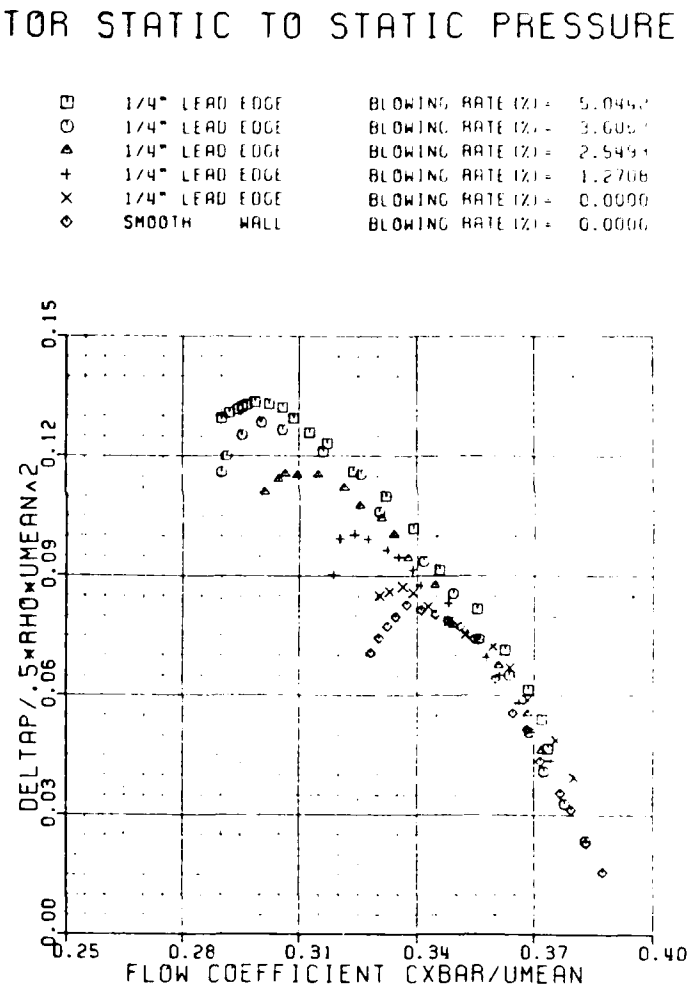

Fig 8 Speedlines: Blowing over front quarter of stator

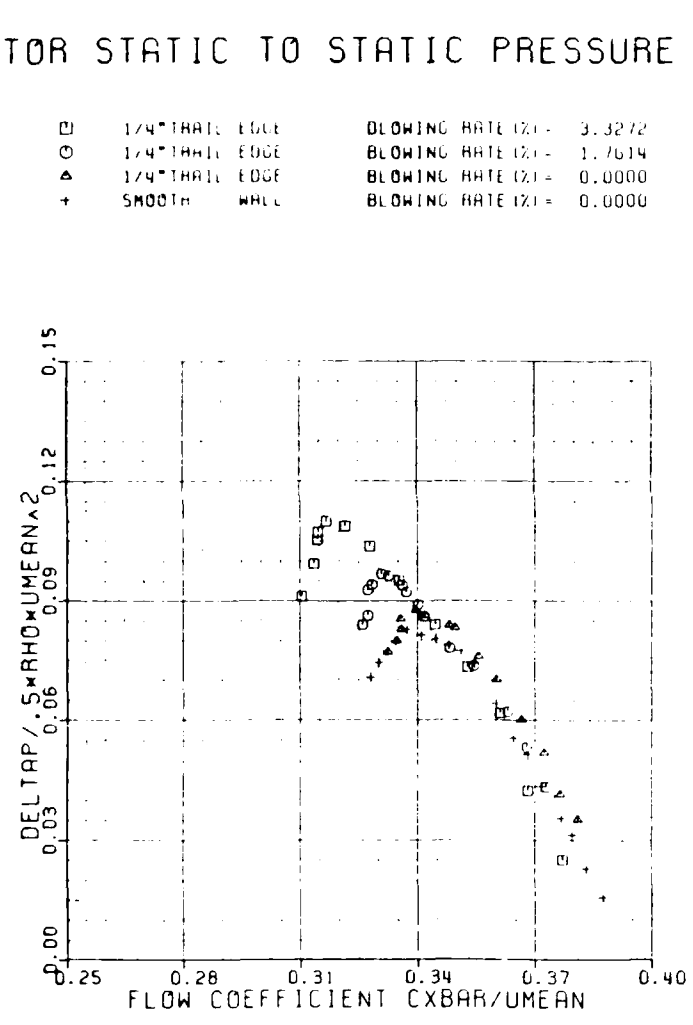

Fig 9 Speedlines: Blowing over rear quarter of stator

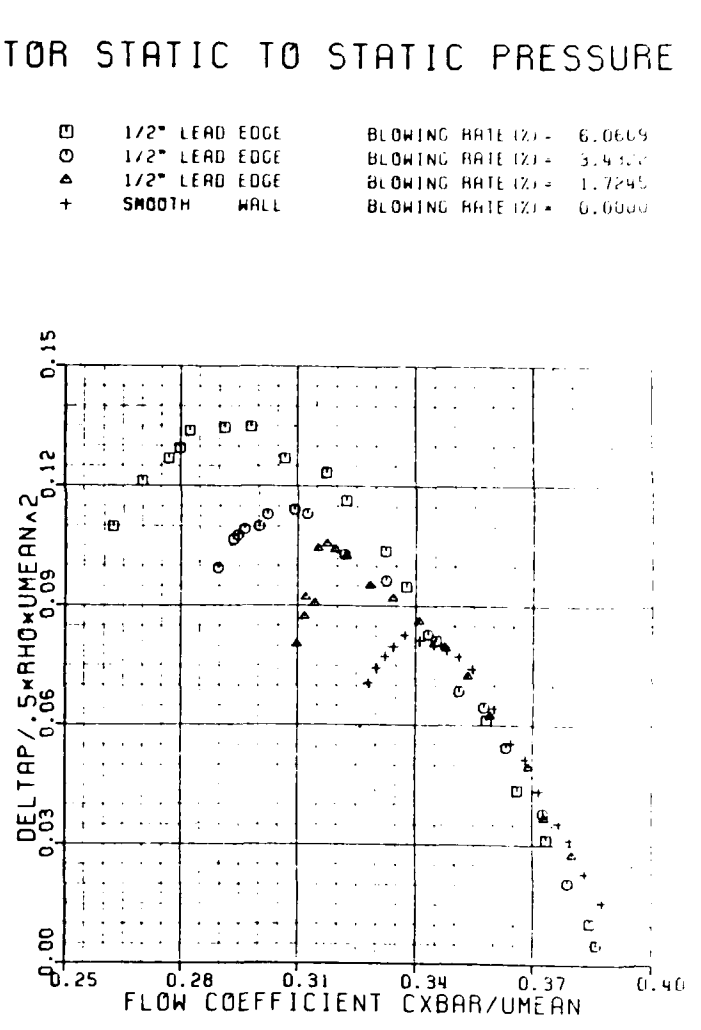

Fig 10 Speedlines: Blowing over front half of stator

PLOT OF INJECTION\REMOVAL RATE VS.
STATIC-TO-STATIC PRESSURE RISE AT STALL

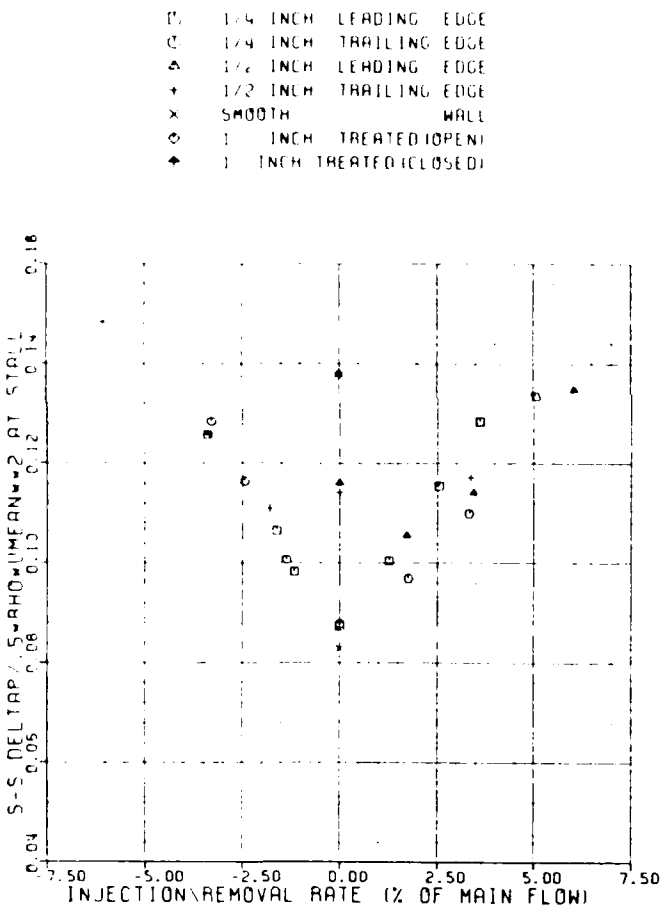

Fig 11 Summary of performance

TASK III: COMPUTATIONAL TECHNIQUES FOR TURBOMACHINES
(Investigators: M.B. Giles, M. Drela, S. Allmaras)

Progress on ISES Design System

In the last year we have made a number of extensions to ISES. When analysing isolated airfoils, the program can now handle supersonic freestreams in addition to subsonic. Although this appears to be a minor change, it has actually been technically non-trivial since it involves the question of what happens to the Kutta condition when the trailing edge flow becomes supersonic. In this case, there is no physical mechanism for ensuring that there is no pressure jump across the trailing edge, and in general there will be such a jump with a shock and expansion fan ensuring that there is no pressure jump across the wake. In normal time-marching codes, there is numerical viscosity which in some ill-defined sense mimics the natural viscosity and establishes the "correct" condition. In our scheme we have no shear viscosity, but have some bulk viscosity in supersonic regions. At subsonic speeds we have to explicitly impose the Kutta condition in exactly the same way as potential methods. Surprisingly, we also have to impose the Kutta condition at supersonic speeds, but in this case what we obtain numerically is a "boundary-layer" type behavior near the trailing edge, and a few cells away from the trailing edge there is an appreciable pressure jump across the airfoil. When analysing cascades the situation becomes further complicated because the inflow and outflow can be in any one of three states: 1) subsonic, 2) supersonic, but axially subsonic, or 3) axially supersonic. Each different state requires different boundary treatments, making the programming implementation much harder than for time-marching methods, but perhaps more rigorously correct.

In addition to the two papers presented at the AIAA 4th Applied Aerodynamic Conference in San Diego in July, which have been sent previously, one

paper will be presented at the AIAA Aerospace Sciences Meeting in Reno in January. This discusses the application of the method to a series of transonic viscous airfoil test cases which has been collected for a workshop, organized by Dr. Pulliam of NASA Ames, which is being held as part of the meeting. An advance copy of the paper will be sent as soon as it is completed.

Progress on the research monograph has been slower than intended due to time limitations. Currently, we are about half-finished and the aim now is to finish over the Christmas/New Year period when there are fewer other commitments.

The ISES program is now being used in industry by Boeing (commercial, military and helicopter divisions), General Electric (Lynn and Cincinnati aero engine divisions), Lockheed (Skunk Works), Northrop (R&D center), and licensing discussions are being held with United Technologies (Sikorsky and Pratt & Whitney) and J. Roncz (an independent consultant who worked with Rutan in designing the Beech Starship). The program is also being used by government research groups at AFWAL (Dr. A. Wennerstrom), NASA Langley, and David Taylor Naval R&D Center (Dr. T. Huang).

Progress on New Research on Unsteady Flow

As discussed in the Research Progress and Forecast Report, we are now redirecting our new efforts into developing methods for calculating unsteady flows in turbomachinery and improving our understanding of these flows in conjunction with the experimental work being performed by the other investigators in the Gas Turbine Laboratory and their associates elsewhere. At present, the computational work is progressing in two areas.

The first area is the development of a new algorithm for unsteady transonic flows, particularly those in which unsteady shock/boundary layer interaction is one of the principal features. Related computational work in

the GTL has shown that the vortex shedding in transonic compressors is due largely to a separated boundary layer on the suction surface which in turn is caused by a normal shock in the blade passage. Low frequency oscillations of the shock have been calculated by an earlier method, at a frequency which is dangerously close to a blade bending frequency and has aroused interest in the engine industry. It is believed that this may be an indication of a shock/b.l. instability similar to those found in transonic diffusers.

The new algorithm is an extension of flux-vector-splitting ideas in which the gradient of the flow variables, as well as the flow variables themselves, are stored at the cell centers. Using the gradients allows one to obtain second order accuracy even on irregular meshes, while using the flux-vector-splitting allows sharply defined shocks without requiring excessive grid resolution. At present, the algorithm has been developed for inviscid flows, but in the future it will be extended to the full Navier-Stokes equations with the intention of calculating shock/b.l. interactions. A paper on this new method is being submitted to the AIAA Computational Fluid Dynamics Meeting in Hawaii next June. A copy of the extended abstract is attached.

The second area is the calculation of turbomachinery flows with vortices. Under funding from Rolls-Royce and ONR, another program has been developed which uses Ni's Lax-Wendroff algorithm to calculate the inviscid flow in a stator or rotor row. The boundary conditions in this program allow one to specify incoming wakes from an upstream blade row and/or incoming isentropic pressure disturbances from an upstream or downstream blade row. One feature is the ability to analyze cases in which the two blade rows have different pitches.

The Rolls Royce/ONR funding is primarily for algorithm development, and so under this multi-investigator grant, in parallel to the experimental work

being performed, we intend to use this program to investigate the importance of vortex shedding on the performance of the next blade row. This will be done by first calculating the unsteady flow due to a wake/rotor interaction, and then repeating the calculation but instead modelling the incoming wake as an unsteady Karman vortex street instead of as a smooth wake. This will allow us to see how important it is to have the correct wake model, which is clearly of interest to both the theoretical analysts who wish to use simple mathematical models and the experimentalists who wish to assign an order of priority to the many interesting questions to be addressed.

A Second Order Flux Split Scheme for the Unsteady 2–D Euler Equations on Arbitrary Meshes

Steven R. Allmaras*
Michael B. Giles†

Computational Fluid Dynamics Laboratory
Department of Aeronautics and Astronautics
Massachusetts Institute of Technology

Abstract

This paper presents an algorithm for solving the unsteady 2–D Euler equations. The scheme uses flux-vector splitting for correct prediction of wave propagation and shock capturing. Grid independent second order accuracy is achieved in a formulation where averages and gradients are stored for each cell. This reduces dissipation due to truncation error. A stability analysis of the linearized 1–D Euler equations is presented for this scheme. Results for steady transonic and supersonic channel flow are also given.

*Research Assistant, Member AIAA

†Assistant Professor, Member AIAA. This work was supported by the Air Force Office of Scientific Research with Dr. J. Wilson as technical monitor

Introduction

Time-marching schemes for the Euler equations have become commonplace. The majority of such schemes have been optimized for steady calculations, but more recently unsteady Euler simulations have received increased interest. In many cases, adequate unsteady simulations cannot be made by removing the time-inaccurate mechanisms (eg. residual smoothing, multigrid, etc.) from a steady-state time-marching scheme. This is because the objectives of an unsteady simulation are different enough to require a new formulation of the solver.

For unsteady Euler simulations it is necessary to have correct wave propagation prediction This is best accomplished by schemes which attempt to directly model the underlying physics of the Euler equations. One such class of schemes is Riemann solvers [4], but these are difficult to extend to general 2-D grids. Another class of schemes uses flux-vector splitting. Included in this class are schemes by Steger and Warming [5] and Anderson, Thomas and van Leer [1]. These methods use the correct domain of dependence for flux calculations, which is more important in unsteady flow than for steady calculations. In supersonic flow, central difference schemes, such as Jameson *et al* [2], and partially upwinded schemes, such as Ni [3], have an enlarged domain of dependence and hence allow information to propagate upstream.

The Euler equations are nondissipative, hence it is desirable to have a scheme with minimal dissipation. This is accomplished by achieving high spatial and temporal accuracy (at least 2^{nd} order). The majority of time-marching schemes in use today assume a Cartesian grid in their formulation and are 2^{nd} order accurate on such grids. However, when they are used on non-Cartesian grids their order of accuracy is reduced, resulting in increased dissipation. For example, the scheme in Ref. [2] uses central differencing of cell averages. Turkel [6] has analytically shown very strict restrictions on grid smoothness for achieving 2^{nd} order accuracy with this scheme in 1-D. He also showed that the scheme becomes inconsistent for highly stretched grids. The schemes of Refs. [1] and [5] use upwind differencing of cell averages, and hence also suffer from these order of accuracy problems.

On the other hand, Ni's node-based scheme [3] uses trapezoidal integration to calculate the flux balance on each cell. For steady-state calculations this is spatially 2^{nd} order accurate (neglecting smoothing) regardless of grid smoothness. Unfortunately, spatial accuracy is reduced for unsteady flows because the distribution step (the discretization of the time derivative term of the Euler equations) assumes a Cartesian grid.

The goals of the present investigation are two-fold. First to develop an unsteady time-marching scheme which gives good wave propagation prediction through the use of flux-vector splitting. Second to reduce dissipation by achieving grid independent 2^{nd} order accuracy in both space and time.

Technical Approach

2–D Euler Equations

The flow of an inviscid compressible fluid is governed by the Euler equations. They represent conservation of mass, momentum, and energy. For 2–D unsteady flow the integral form is

$$\frac{\partial}{\partial t}\iint_{\Omega} \mathbf{U}\, dA + \oint_{\partial\Omega} (\mathbf{F}\, dy - \mathbf{G}\, dx) = 0, \tag{1}$$

where the integrals are taken over a control volume Ω bounded by the curve $\partial\Omega$. The conservation variables $\mathbf{U}$ and the Cartesian flux functions $\mathbf{F}$ and $\mathbf{G}$ are given by

$$\mathbf{U} = \begin{pmatrix} \rho \\ \rho u \\ \rho v \\ e \end{pmatrix} \qquad \mathbf{F} = \begin{pmatrix} \rho u \\ \rho u^2 + P \\ \rho uv \\ \rho u h_0 \end{pmatrix} \qquad \mathbf{G} = \begin{pmatrix} \rho v \\ \rho uv \\ \rho v^2 + P \\ \rho v h_0 \end{pmatrix}, \tag{2}$$

where ρ is density, $\vec{q} = u\vec{\imath} + v\vec{\jmath}$ is the velocity, P is pressure, e is total internal energy per unit volume and h_0 is total enthalpy. Closure of the system is obtained by the equation of state for a perfect gas,

$$P = (\gamma - 1)\left[e - \frac{1}{2}\rho(u^2 + v^2)\right], \tag{3}$$

where γ is the specific heat ratio (for air $\gamma = 1.40$). The total enthalpy relation is then given by $\rho h_0 = e + P$.

Spatial Discretization

The spatial discretization for this scheme originally came from a Godunov-type method by van Leer [7] for the 1–D wave equation. Within each cell the solution is assumed linear.

$$\mathbf{U}(x, y) = \overline{\mathbf{U}} + (x - x_c)\overline{\mathbf{U}_X} + (y - y_c)\overline{\mathbf{U}_Y} \tag{4}$$

where $\overline{\mathbf{U}}$ is the solution average over the cell, and $(\overline{\mathbf{U}_X}, \overline{\mathbf{U}_Y})$ is the average gradient for the cell. These may be associated with the cell centroid (x_c, y_c) defined by

$$x_c \equiv \frac{\iint x\, dA}{\iint dA} \qquad y_c \equiv \frac{\iint y\, dA}{\iint dA} \tag{5}$$

With this intracell distribution, the solution is not necessarily continuous at cell faces.

Substituting this linearized solution into the Euler equations and integrating over the cell area gives an equation for the time evolution of the cell averages.

$$\frac{\partial}{\partial t}\left(A\overline{\mathbf{U}}\right) + \sum_m \vec{\mathbf{H}}(\mathbf{U}_m)\cdot\vec{n}\Delta s = 0, \qquad \vec{\mathbf{H}} = \mathbf{F}\vec{\imath} + \mathbf{G}\vec{\jmath} \tag{6}$$

where A is the cell area, $\vec{n}$ the outward normal and Δs the length of each face of the cell. The fluxes through the faces $\vec{\mathbf{H}}(\mathbf{U}_m)$ are evaluated at the midpoints of the cell faces as shown in Fig. 1. If $\mathbf{U}_m$ is known to 2^{nd} order at each face midpoint, then Eq. 6 is 2^{nd} order accurate regardless of grid smoothness.

This finite volume formulation of the discrete Euler equations is conservative, which gives the correct shock jump relations and shock velocity for unsteady flows.

Flux-vector Splitting

The fluxes through the faces are obtained using flux-vector splitting. In 1-D the flux $\mathbf{F}$ is separated into two components: a forward flux ($\mathbf{F}^+$) and a backward flux ($\mathbf{F}^-$). At a given point, $\mathbf{F}^+$ is evaluated using solution information extrapolated from the left, and $\mathbf{F}^-$ is evaluated using right extrapolated information. This is illustrated in Fig. 2 where the flux through the face at $i+1/2$ is given by

$$\mathbf{F}_{i+1/2} = \mathbf{F}^+(\mathbf{U}^-_{i+1/2}) + \mathbf{F}^-(\mathbf{U}^+_{i+1/2}) \tag{7}$$

where the extrapolated solutions are obtained using average and gradient information from the two adjacent cells.

$$\mathbf{U}^-_{i+1/2} = \overline{\mathbf{U}}_i + (x_{i+1/2} - x_i)\overline{\mathbf{U}_X}_i, \qquad \mathbf{U}^+_{i+1/2} = \overline{\mathbf{U}}_{i+1} + (x_{i+1/2} - x_{i+1})\overline{\mathbf{U}_X}_{i+1} \tag{8}$$

These extrapolated solutions are 2^{nd} order accurate as long as the gradients are known to at least 1^{st} order.

The flux splitting used is that developed by van Leer [8]. In supersonic flow the split fluxes are given by

$$\begin{aligned} \mathbf{F}^+ &= \mathbf{F}, \quad \mathbf{F}^- = 0 \qquad M \geq +1 \\ \mathbf{F}^+ &= 0, \quad \mathbf{F}^- = \mathbf{F} \qquad M \leq -1 \end{aligned} \tag{9}$$

In subsonic flow ($|M| < 1$) they are given by

$$\mathbf{F}^\pm = \begin{pmatrix} \pm\frac{\rho c}{4}(1 \pm M)^2 \\ f_1^\pm c \left\{ \dfrac{(\gamma - 1)M \pm 2}{\gamma} \right\} \\ f_1^\pm c^2 \left\{ \dfrac{[(\gamma - 1)M \pm 2]^2}{2(\gamma^2 - 1)} \right\} \end{pmatrix} \tag{10}$$

The 2-D extension of this scheme is accomplished by rotating the fluxes normal to the face. The splitting is then based on the normal Mach number defined as

$$M_n = (\vec{q}/c) \cdot \vec{n}, \qquad M_s = (\vec{q}/c) \cdot \vec{s} \tag{11}$$

where $\vec{n}$ is the outward normal to the cell. For completeness, the tangential Mach number is also given. In the face normal coordinates, the subsonic split fluxes are given as

$$\vec{\mathbf{H}}^{\pm} \cdot \vec{n} = \begin{pmatrix} \pm\frac{\rho c}{4}(1 \pm M_n)^2 \\ h_1^{\pm} c \left\{ \frac{(\gamma-1)M_n \pm 2}{\gamma} \right\} \\ h_1^{\pm} c M_s \\ h_1^{\pm} c^2 \left\{ \frac{[(\gamma-1)M_n \pm 2]^2}{2(\gamma^2-1)} + \frac{M_s^2}{2} \right\} \end{pmatrix} \tag{12}$$

where the second and third entries are normal and tangential momentum, respectively.

Gradient Equations

There are several options for calculating the gradients ($\overline{\mathbf{U}_X}$, $\overline{\mathbf{U}_Y}$) on each cell. One method is to central difference the cell averages. This is simple but has the wrong domain of dependence in supersonic flow, allowing information to propagate upstream. This counteracts the use of flux splitting to calculate the cell averages. Also this method is unconditionally unstable.

Another option is to update the gradients by minimizing the solution jump at cell faces. For a uniform grid in 1-D this works out to be

$$\overline{\mathbf{U}_{X_i}}^{n+1} = \frac{1}{\Delta x}\left\{ (\overline{\mathbf{U}}^n_{i+1} - \frac{1}{2}\Delta x \overline{\mathbf{U}_{X_{i+1}}}^n) - (\overline{\mathbf{U}}^n_{i-1} + \frac{1}{2}\Delta x \overline{\mathbf{U}_{X_{i-1}}}^n) \right\} \tag{13}$$

For steady-state calculations, this is a simple and efficient approach; however, it gives poor wave propagation predictions. Like central differencing it allows information to propagate upstream in supersonic flow.

A third option is to evolve the gradients in time along with the cell averages by taking the moment of the Euler equations as suggested in Ref. [7]. If properly discretized this method gives the same domain of dependence as the average equations, which leads to proper wave propagation prediction.

The derivation of the gradient equations is first shown for 1-D. The moment equations are obtained by first multiplying the 1-D Euler equations by x.

$$x\left\{ \frac{\partial \mathbf{U}}{\partial t} + \frac{\partial \mathbf{F}}{\partial x} = 0 \right\} \quad \rightarrow \quad \frac{\partial (x\mathbf{U})}{\partial t} + \frac{\partial (x\mathbf{F})}{\partial x} - \mathbf{F} = 0 \tag{14}$$

Next, the linearized solution is substituted into Eq. 14 and integrated over the cell ($x = -\Delta x/2$ to $+\Delta x/2$). When this is done, the cell average in the time derivative term vanishes, giving

$$\frac{\partial}{\partial t}\left[\frac{\Delta x^3}{12} \overline{\mathbf{U}_X} \right] + x\mathbf{F}\Big|_{-\Delta x/2}^{+\Delta x/2} - \Delta x \mathbf{F}(\overline{\mathbf{U}}) = 0 \tag{15}$$

In this equation the third term is obtained by assuming $\mathbf{F}(\mathbf{U})$ is linear within the cell.

$$\mathbf{F}(\mathbf{U}) = \mathbf{F}(\overline{\mathbf{U}}) + x \frac{\partial \mathbf{F}}{\partial \mathbf{U}}_{x=0} \overline{\mathbf{U}_X} + O(\Delta x^2) \tag{16}$$

To 2^{nd} order accuracy the second term is given by

$$(x\mathbf{F})_{i+1/2} = \left(x_{i+1/2} - x_i\right)\left\{\mathbf{F}^+(\overline{\mathbf{U}}_i + (x_{i+1/2} - x_i)\overline{\mathbf{U}_X}_i) + \mathbf{F}^-(\overline{\mathbf{U}}_{i+1} + (x_{i+1/2} - x_{i+1})\overline{\mathbf{U}_X}_{i+1})\right\} \tag{17}$$

Note that the term in brackets is the flux through the face evaluated for the cell average equations. Hence, the rather expensive operation of calculating fluxes through the faces need not be repeated for the gradient equations.

Ref. [7] notes that calculating the gradients by the moment equation results in a linearized approximation which gives the integrated least square error from the exact solution within each cell.

In two dimensions the x and y moment equations result in a coupled system for the cell gradients $(\overline{\mathbf{U}_X}, \overline{\mathbf{U}_Y})$. The full semi-discrete scheme in 2-D is then given by

$$\begin{aligned}
\frac{\partial}{\partial t}\left(A\overline{\mathbf{U}}\right) &= -\sum \vec{\mathbf{H}}_m \cdot \vec{n}\Delta s \\
\frac{\partial}{\partial t}\left(A_{yy}\overline{\mathbf{U}_X} + A_{xy}\overline{\mathbf{U}_Y}\right) &= -\sum (x_m - x_c)\vec{\mathbf{H}}_m \cdot \vec{n}\Delta s + A\mathbf{F}(\overline{\mathbf{U}}) \\
\frac{\partial}{\partial t}\left(A_{xy}\overline{\mathbf{U}_X} + A_{xx}\overline{\mathbf{U}_Y}\right) &= -\sum (y_m - y_c)\vec{\mathbf{H}}_m \cdot \vec{n}\Delta s + A\mathbf{G}(\overline{\mathbf{U}})
\end{aligned} \tag{18}$$

where A_{xx}, A_{yy} and A_{xy} are second area moments about the cell centroid.

$$A_{yy} = \iint (x - x_c)^2\, dA, \quad A_{xx} = \iint (y - y_c)^2\, dA, \quad A_{xy} = \iint (x - x_c)(y - y_c)\, dA \tag{19}$$

Note that if the gradients are neglected, the resulting scheme is identical to the 1^{st} order upwinded option in the scheme of Ref. [1].

Time Integration

The semi-discrete equations are integrated in time using an explicit 3-stage Runge-Kutta scheme. Given the nonlinear O.D.E.

$$\frac{\partial u}{\partial t} = f(u,t) \tag{20}$$

the solution $u(t)$ is evolved in time by

$$\begin{aligned}
u^0 &= u^n \\
u^1 &= u^0 + \alpha\Delta t f^0 \\
u^2 &= u^0 + 1/2\Delta t f^1 \\
u^3 &= u^0 + \Delta t f^2 \\
u^{n+1} &= u^3
\end{aligned} \tag{21}$$

This scheme is 2^{nd} order accurate in time independent of the value of the first stage integration constant α. Thus α is a free parameter which can be used to maximize the time step Δt.

Stability Analysis

The stability of this scheme is analyzed using the linearized 1-D Euler equations rather than the simple scalar wave equation. This is because the greatest stability restriction occurs in subsonic flow, where the Euler equations have mixed eigenvalues. Also, the effect of the split flux vectors is not easily obtained from the wave equation. These matters are complicated by the coupling between the average and gradient equations.

The linearized 1-D Euler equations are given by

$$\frac{\partial \mathbf{U}}{\partial t} + \mathbf{A}\frac{\partial \mathbf{U}}{\partial x} = 0, \qquad \mathbf{A} \equiv \frac{\partial \mathbf{F}}{\partial \mathbf{U}} \tag{22}$$

A single stage of the discretized form of the average and gradient equations on a uniform grid is then given by

$$\begin{aligned} \overline{\mathbf{U}}_j^k = \overline{\mathbf{U}}_j^0 - \alpha_k \frac{\Delta t}{\Delta x} \Big\{ &\left[\mathbf{A}^+(1-T^{-1}) + \mathbf{A}^-(T-1)\right] \overline{\mathbf{U}}_j^{k-1} \\ &+ \frac{1}{2}\left[\mathbf{A}^+(1-T^{-1}) - \mathbf{A}^-(T-1)\right] \overline{\Delta \mathbf{U}}_j^{k-1} \Big\} \end{aligned} \tag{23}$$

$$\begin{aligned} \overline{\Delta \mathbf{U}}_j^k = \overline{\Delta \mathbf{U}}_j^0 - 6\alpha \frac{\Delta t}{\Delta x} \Big\{ &\left[\mathbf{A}^+(1+T^{-1}) + \mathbf{A}^-(T+1) - 2\mathbf{A}\right] \overline{\mathbf{U}}_j^{k-1} \\ &+ \frac{1}{2}\left[\mathbf{A}^+(1+T^{-1}) - \mathbf{A}^-(T+1)\right] \overline{\Delta \mathbf{U}}_j^{k-1} \Big\} \end{aligned} \tag{24}$$

where $\overline{\Delta \mathbf{U}} \equiv \Delta x \overline{\mathbf{U}_X}$ and T is the translation operator ($T\mathbf{U}_j = \mathbf{U}_{j+1}$). In addition the split flux Jacobians are defined as

$$\mathbf{A}^{\pm} \equiv \frac{\partial \mathbf{F}^{\pm}}{\partial \mathbf{U}} \tag{25}$$

The Fourier mode to be examined is

$$\mathbf{Q}_j^n = \begin{pmatrix} \overline{\mathbf{U}}_j^n \\ \overline{\Delta \mathbf{U}}_j^n \end{pmatrix} = \hat{\mathbf{Q}}^n e^{ij\theta}, \qquad -\pi \le \theta \le +\pi \tag{26}$$

where $\hat{\mathbf{Q}}$ is a 6×1 constant vector. Substitution of this into Eqs. 23 and 24 results in the matrix equation

$$\hat{\mathbf{Q}}^{n+1} = \mathbf{G}\hat{\mathbf{Q}}^n \tag{27}$$

where $\mathbf{G}$ is the amplification matrix whose eigenvalues must have magnitudes less that one for stability. For a given Mach number, α, θ and CFL number defined by

$$\lambda = (u + c)\frac{\Delta t}{\Delta x} \tag{28}$$

the eigenvalues of $\mathbf{G}$ are calculated by EISPACK.

Figure 3 shows the effect of the first stage integration constant α on the stability boundary for the 1st order scheme (Eq. 23 only with no gradients). For supersonic flow the maximum CFL is $\lambda = 2$ at $\alpha \approx 0.17$, but the stability boundary is sensitive to the choice of α. For subsonic flow the

maximum CFL decreases to $\lambda = 1.9$ at $M = 0$. As a comparison, the maximum CFL for a 3-stage central differenced scheme is $\lambda = 2$ independent of Mach number.

The stability boundary for the full 2nd order scheme (Eqs. 23 and 24) is shown in Fig. 4. For supersonic flow, the maximum CFL number is $\lambda = 0.59$ at $\alpha \approx 0.17$ and decreases as $M \to 0$. Again, the maximum CFL is sensitive to the choice of α. A linear curve fit for the maximum CFL is then given by

$$\lambda_{\max} = \begin{cases} 0.51 + 0.08M & M < 1 \\ 0.59 & M \geq 1 \end{cases} \tag{29}$$

Shock Capturing

As shown in Ref. [8], the 1st order upwinded scheme (ie. averages only) captures shocks with at most two interior cells with no additional dissipation. Unfortunately, this is not also true for the full 2nd order scheme. In the immediate vicinity of shocks the gradients must be limited or turned off. This is done by adding an exponential decay term to the gradient equations. If $\mathbf{R}_X$ is the residual for the x moment equation in 1-D, then the modified equation is

$$\overline{\mathbf{U}_{X_j}}^k = \overline{\mathbf{U}_{X_j}}^0 - \alpha_k \frac{\Delta t}{\Delta x^3/12} \left\{ \mathbf{R}_X + \epsilon \frac{\Delta x^3/12}{\Delta t} \frac{|\delta^2 \overline{\rho}|}{\overline{\rho}} \overline{\mathbf{U}_{X_j}}^0 \right\}, \qquad \epsilon \approx 5 \tag{30}$$

The decay term contains a switch to turn it on only in the vicinity of shocks. This switch is the second difference of average density. In smooth flow, $|\delta^2 \rho| \sim O(\Delta x^2)$ and the source term is 2nd order. In the vicinity of shocks, where $|\delta^2 \rho| \sim 1$, the source term gives zeroth order accurate gradients and a 1st order solution.

Results

In this section results are shown for transonic and supersonic flow over a bi-circular arc cascade, also known as Ni's Bump. These are standard test cases for 2-D Euler solvers. In addition, an order of accuracy study is conducted for the present scheme.

Transonic Ni Bump

The first test case is a transonic 20% bi-circular arc cascade with an inlet Mach number of 0.675. The computational grid, shown in Fig. 5, is 64 by 16 cells and is algebraically generated. The solution on this grid is shown in Figs. 6, 7 and 8. Figure 6 is a plot of Mach number distribution on the upper and lower walls of the channel. As the plot shows, the shock on the lower wall is captured with only one interior cell. Note also the absence of any pre or post-shock oscillations or overshoots. Figure 7 shows Mach number contours for the channel interior; throughout the domain

the solution is smooth. Typically, for Euler solvers oscillations in density near shocks and other strong gradients are much more acute than for Mach number. Figure 8 shows that the density is also smooth throughout the domain, even near the shock.

Supersonic Ni Bump

The same series of plots is shown for a supersonic 4% bi-circular arc cascade with inlet Mach number of 1.4. The grid for this case (Fig. 9) is 56×16 cells. It has the same distribution as that for the transonic case, except that cells have been deleted from the forward section where the flow should be uniform. The Mach number plots in Figs. 10 and 11 show oblique shocks generated at the leading and trailing edges of the arc, which reflect off the upper wall. Fig. 10 shows that the lower wall shocks are captured with one interior cell. However, by the time the leading edge shock impinges on the upper wall, it is smeared with three interior cells. This is believed to be due to cross-stream dissipation introduced by the split fluxes.

Order of Accuracy Study

The order of accuracy of the present scheme is verified using a completely subsonic channel flow ($M_{\text{inlet}} = 1/2$). The arc of the previous cases is replaced by a 10% $\sin^2 x$ bump, which smoothly blends into the straight portions of the lower wall. This eliminates leading and trailing edge stagnation points and their associated large truncation errors. Also no shock losses occur since the flow is subsonic. Hence, all losses for this case are purely numerical. In this study, RMS of total pressure loss over the domain is used as a measure of these numerical losses. It is defined as

$$||1 - P_T/P_{T\infty}||_2 = \sqrt{\frac{\sum_{i,j}(1 - P_{Tij}/P_{T\infty})^2}{\sum_{i,j} 1}} \tag{31}$$

$$P_T = P(1 + \frac{\gamma - 1}{2} M^2)^{\frac{\gamma}{\gamma - 1}} \tag{32}$$

Total pressure loss has been found in the past to be a good indicator of accuracy for Euler solvers.

Figure 13 shows the finest grid (64×16) used in this study. Coarser grids (32×8, 16×4 and 8×2) are obtained by deleting every other grid line from the next finer grid. As before these grids are algebraically generated. Figure 14 shows the losses for both the 1st and 2nd order schemes along with Jameson's central difference scheme [2] on these grids. The slope of each line is the scheme's order of accuracy. The slope for the present scheme using averages only is 0.63, indicating that in this norm the scheme is not even 1st order accurate. The full scheme using both averages and gradients (Eqs. 18) is truely 2nd order, having a slope of 2.1. For comparison, the central difference scheme is also plotted. Even though the grids are fairly smooth, this scheme fails to obtain 2nd order accuracy, since the slope of its line is only 1.4. It is expected that the central difference

scheme will further decrease in accuracy as the grid is made less smooth, while the present scheme will remain unconditionally 2^{nd} order accurate.

For solutions on the 64×16 grid, the present 2^{nd} order scheme has approximately 10% the total pressure error of the central difference scheme and about 1% that of the 1^{st} order scheme using averages only.

Summary

The new developments of the present investigation to be discussed in full in the final paper include the following:

A new time-marching algorithm for the unsteady 2–D Euler equations is presented. The scheme utilizes flux-vector splitting for shock capturing and correct prediction of wave propagation. Grid independent 2^{nd} order accuracy is achieved in a formulation where averages and gradients are stored for each cell. This more closely models the nondissipative nature of the Euler equations, by reducing truncation error on non-uniform grids.

A stability analysis of the linearized 1–D Euler equations is conducted for this scheme. Using explicit 3-stage Runge-Kutta time integration, the maximum CFL number for the spatially 2^{nd} order scheme is found to be approximately 1/4 that for the spatially 1^{st} order scheme. In subsonic flow, the use of flux-vector splitting results in a slightly lower CFL restriction.

Results for steady transonic and supersonic channel flow are presented. The final paper will include studies of shock motion for unsteady channel flows.

References

[1] Anderson, W. K., Thomas, J. L., and van Leer, B., "A Comparison of Finite Volume Flux Vector Splittings for the Euler Equations," AIAA Paper 85-0122, January 1985.

[2] Jameson, A., Schmidt, W., and Turkel, E., "Numerical Solutions of the Euler Equations by Finite Volume Methods Using Runge-Kutta Time-Stepping Schemes," AIAA Paper 81-1259, June 1981.

[3] Ni, R. H., "A Multiple-Grid Scheme for Solving the Euler Equations," *AIAA Journal*, Vol. 20, No. 11, November 1981, pp. 1565–1571.

[4] Roe, P. L., *J. Computational Phys.* **43** p. 357, 1981.

[5] Steger, J. L., and Warming, R. F., "Flux Vector Splitting of the Inviscid Gasdynamic Equations with Application to Finite Difference Methods," *J. Computational Phys.* **40**, pp. 263-293, 1981.

[6] Turkel, E., "Accuracy of Schemes for the Euler Equations with Non-Uniform Meshes," AIAA Paper 86-0341, January 1986.

[7] van Leer, B., "Towards the Ultimate Conservative Difference Scheme. IV. A New Approach to Numerical Convection," *J. Computational Phys.* **23**, pp. 276-299, 1977.

[8] van Leer, B., "Flux-vector Splitting for the Euler Equations," ICASE Report No. 82-30, September 1982.

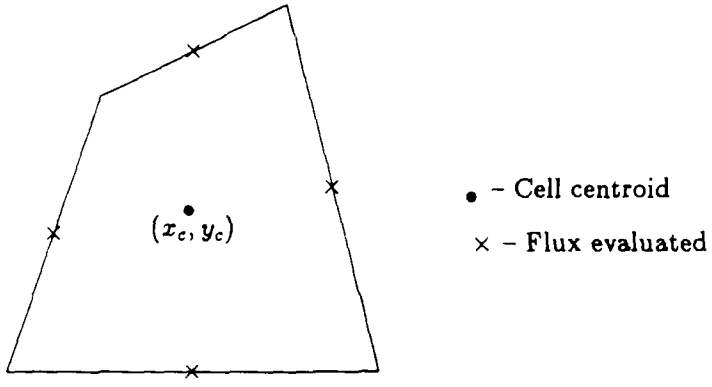

Figure 1: Typical conservation cell

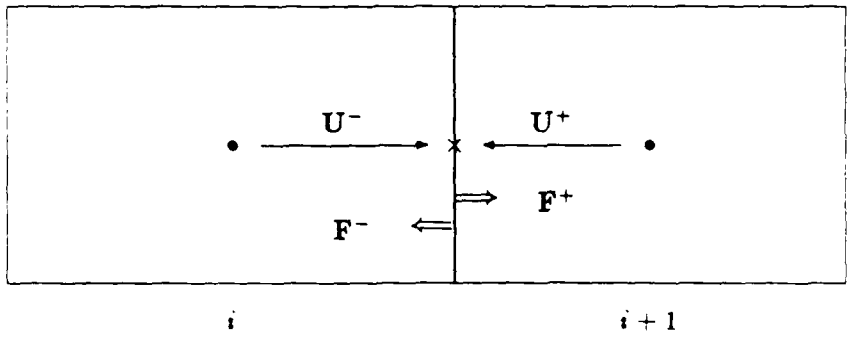

Figure 2: Flux-vector splitting in 1-D

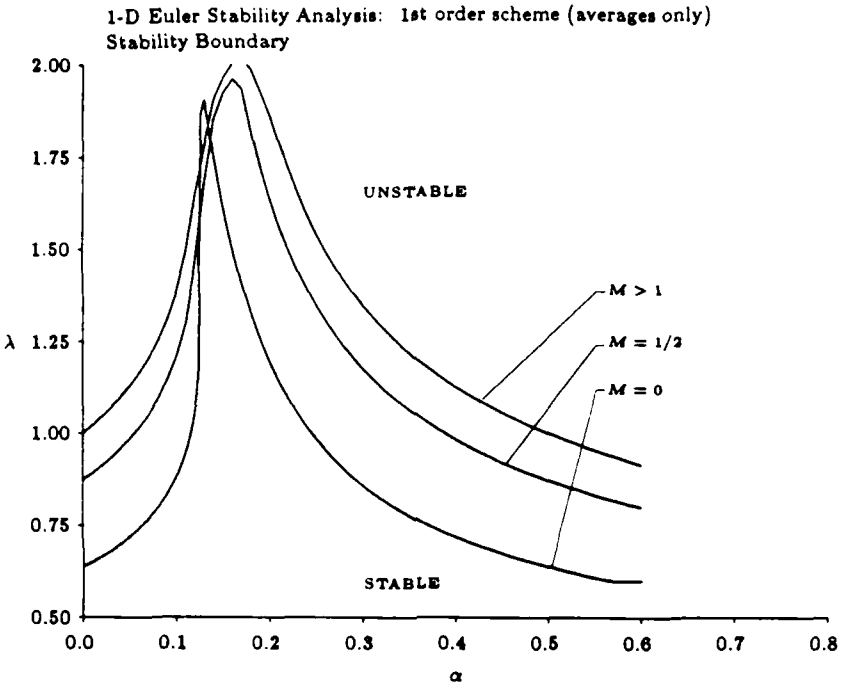

Figure 3: Effect of first stage integration constant on stability boundary of 1st order scheme

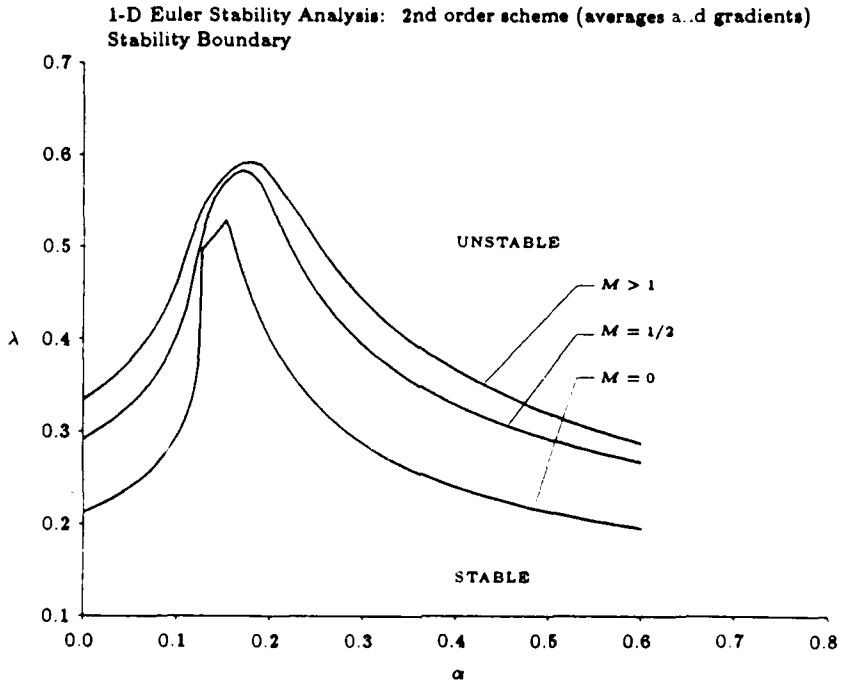

Figure 4: Effect of first stage integration constant on stability boundary of 2nd order scheme

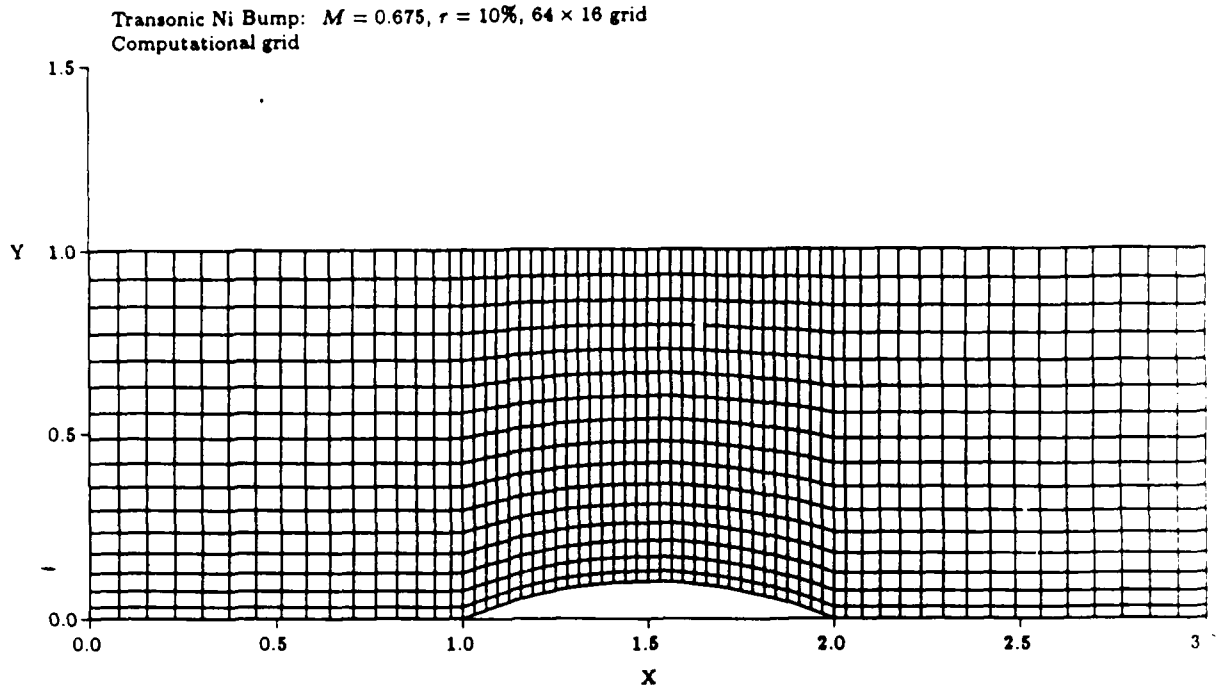

Figure 5: Computational grid for transonic Ni bump ($M = 0.675$, $\tau = 10\%$)

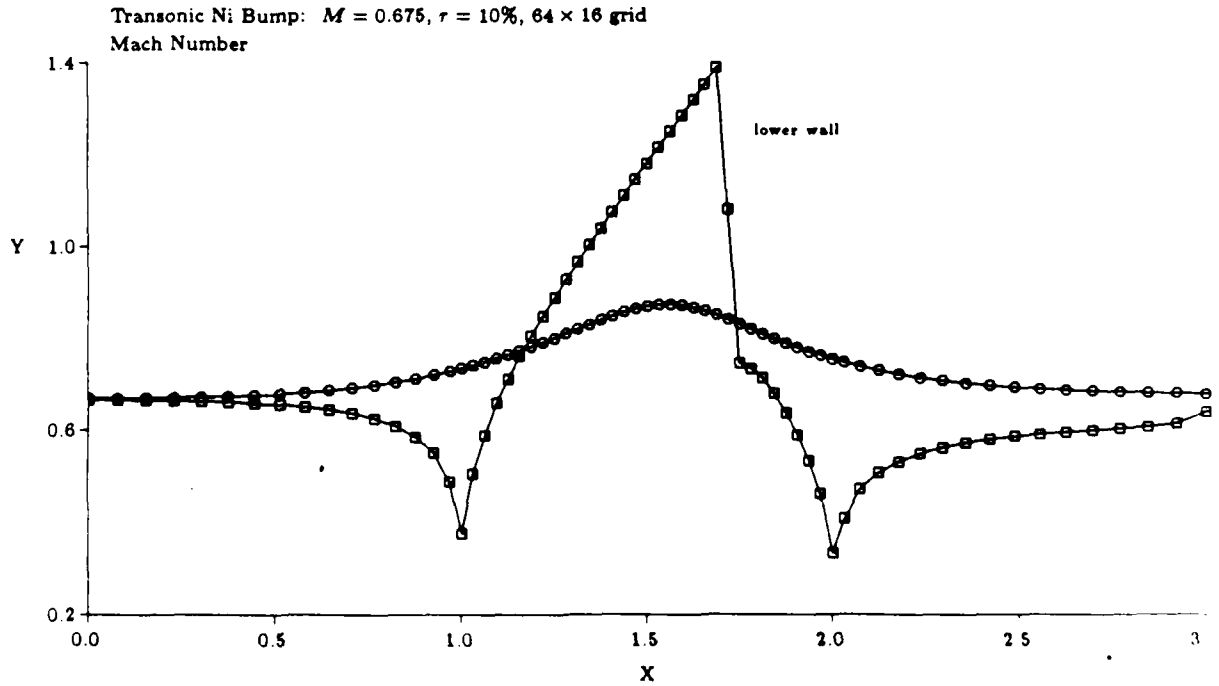

Figure 6: Mach number distribution on upper and lower walls for transonic Ni bump

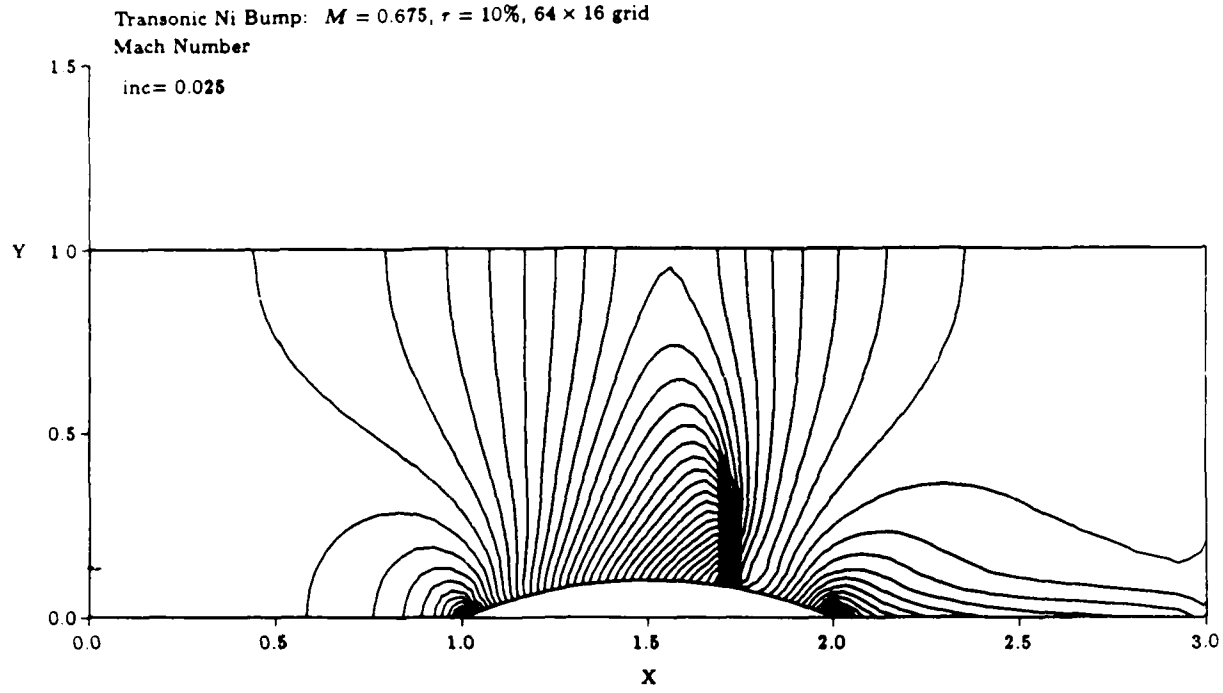

Figure 7: Mach number contours for transonic Ni bump ($\Delta M = 0.025$)

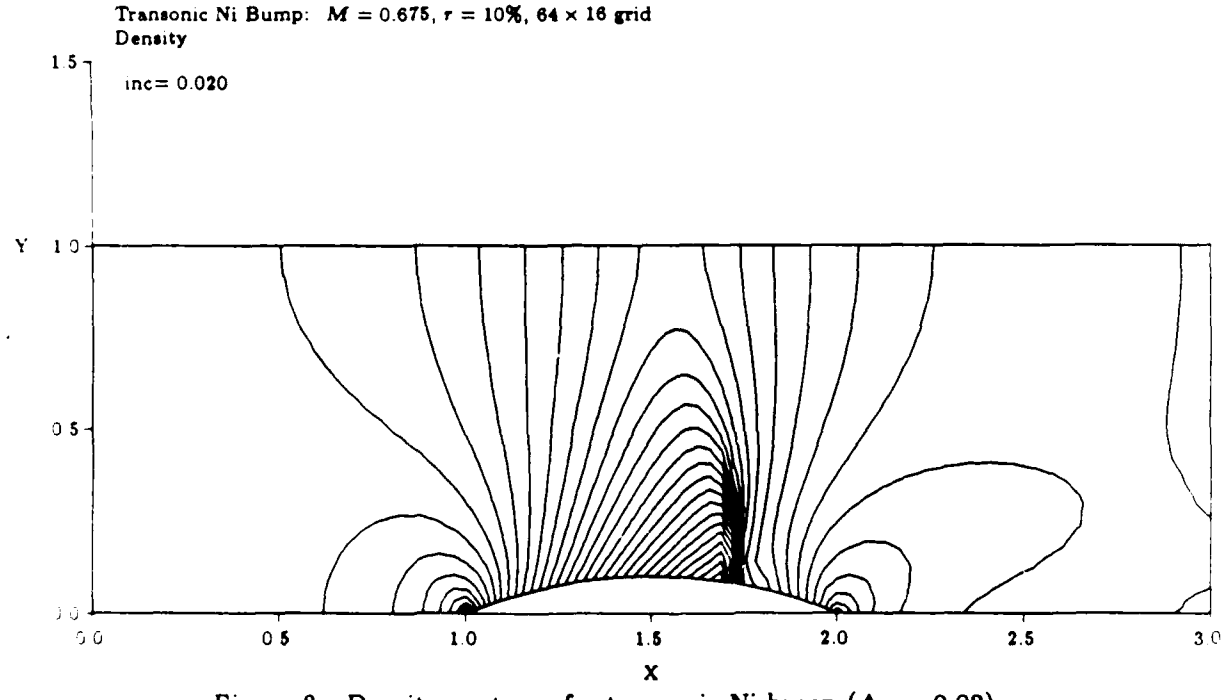

Figure 8: Density contours for transonic Ni bump ($\Delta \rho = 0.02$)

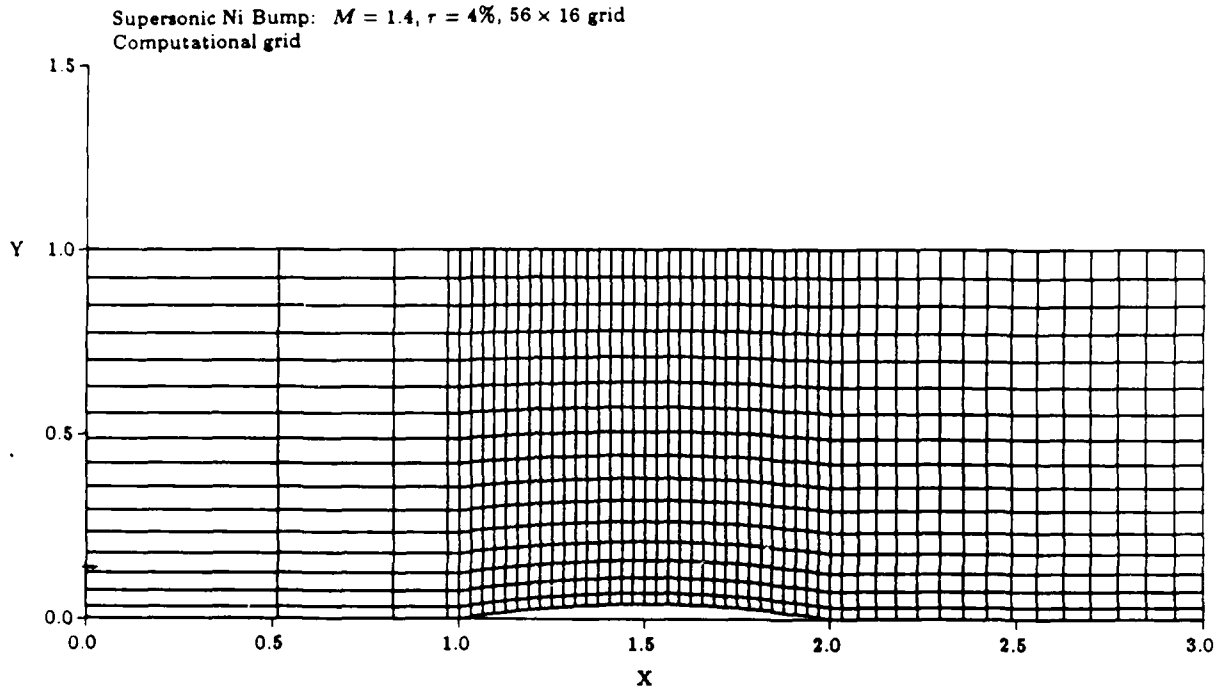

Figure 9: Computational grid for supersonic Ni bump ($M = 1.4$, $\tau = 4\%$)

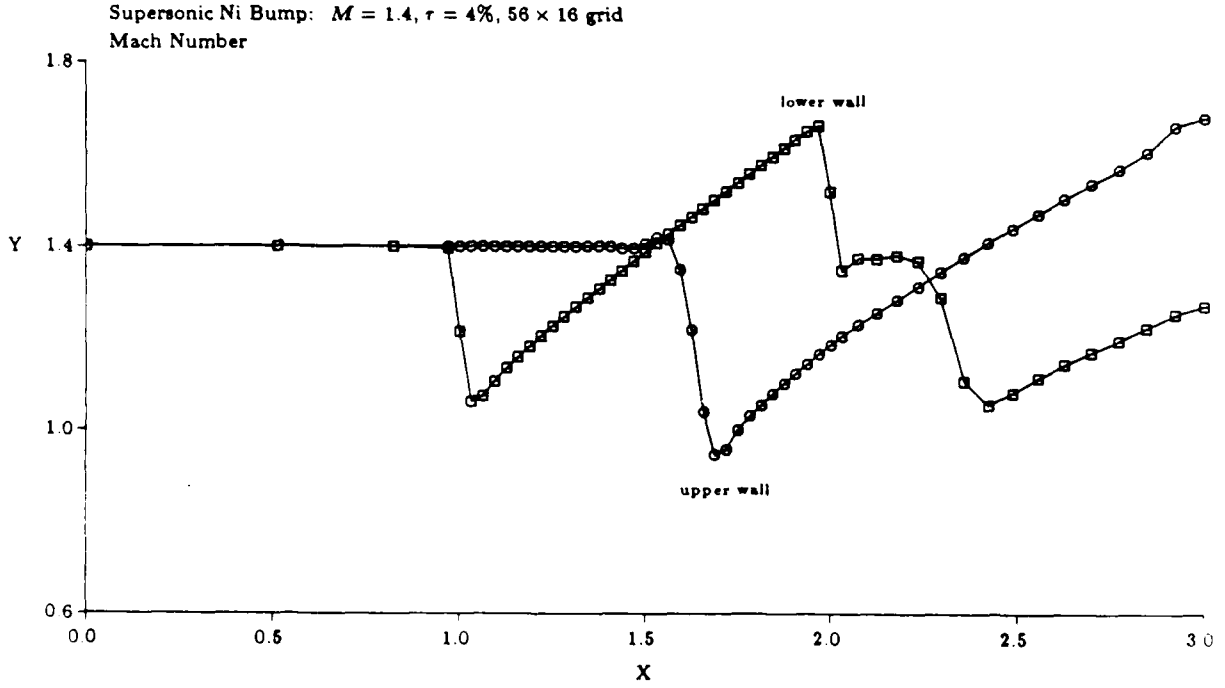

Figure 10: Mach number distribution on upper and lower walls for supersonic Ni bump

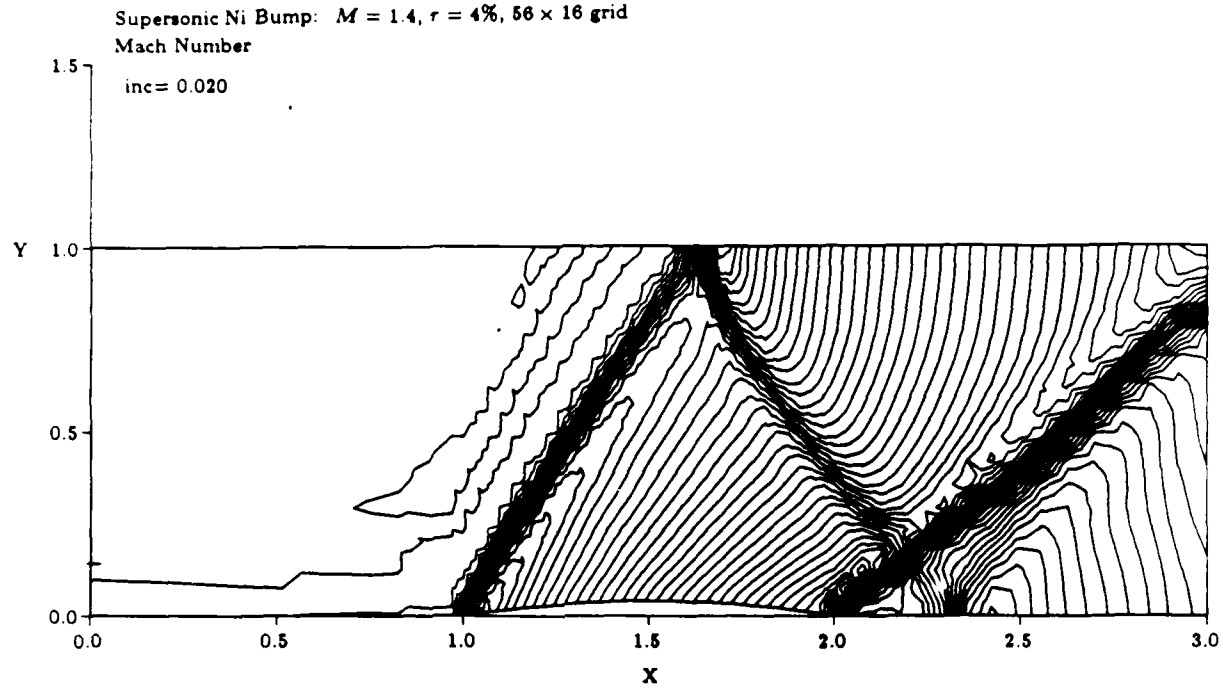

Figure 11: Mach number contours for supersonic Ni bump ($\Delta M = 0.02$)

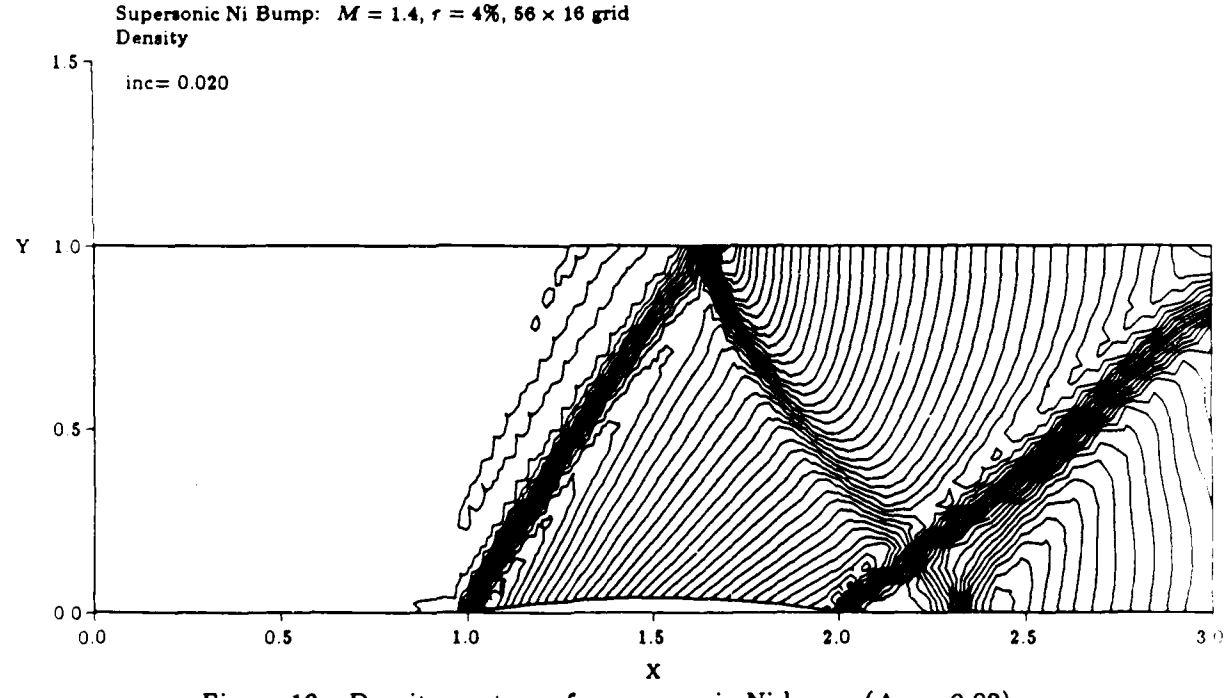

Figure 12: Density contours for supersonic Ni bump ($\Delta \rho = 0.02$)

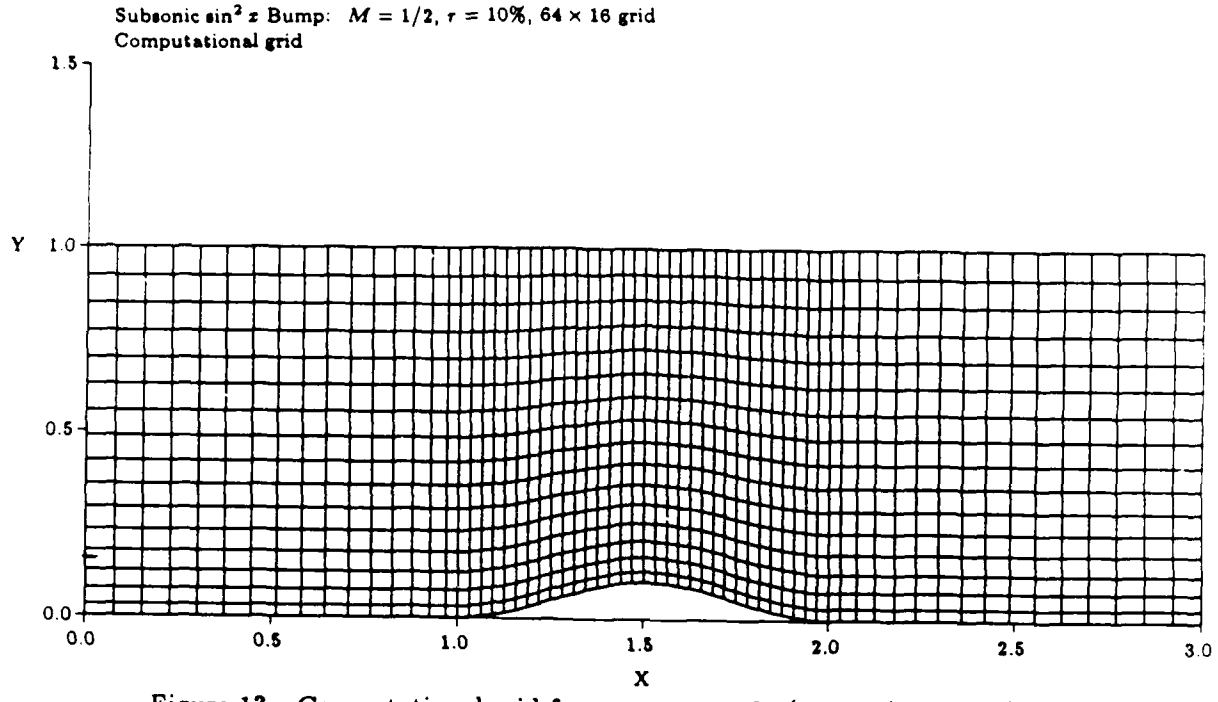

Figure 13: Computational grid for accuracy study ($M = 1/2$, $\tau = 10\%$)

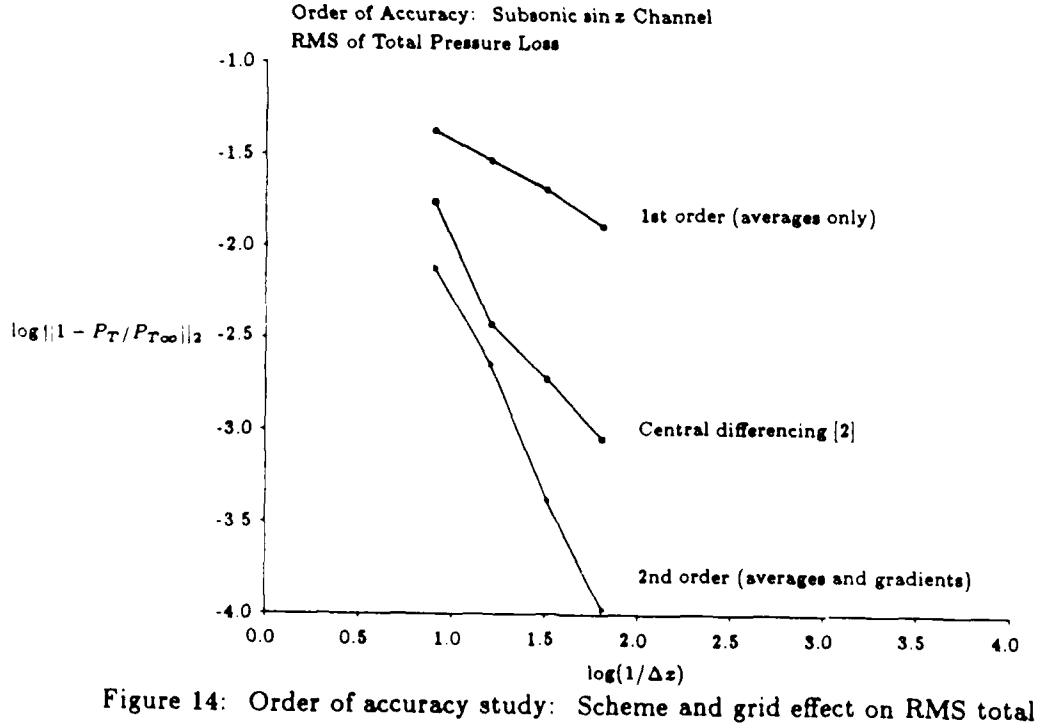

Figure 14: Order of accuracy study: Scheme and grid effect on RMS total pressure error

TASK IV: THEORETICAL MODELLING OF STABILITY AND UNSTEADINESS IN TRANSONIC COMPRESSOR FLOW FIELDS

(Investigators: J.E. McCune, E. Imperatori)

Introduction (Foreward)

This report continues the theme of its predecessor (November 1985) in discussing recent progress in understanding unsteady effects in turbomachines, especially in transonic compressors. As reported previously, unsteady vortex patterns, similar to "vortex streets", can form behind a blade row. These were shown to lead to "temperature separation" -- a total temperature depression in the time-averaged wake behind each blade -- providing a partial explanation of recent experimental observations in transonic machines. Entropy spottiness may also occur.

(This Task's schedule was delayed somewhat in the past months due to time needed by the principal investigator to recover from surgery. The delay is currently being made up, and we expect to be back "on schedule" before Christmas.)

Imbedded Flows and Convected Patterns

In steady or quasi-steady flow past airfoils, the phenomenon of separation and reattachment of the boundary layer -- leading to so-called separation "bubbles" -- is relatively familiar. The flow within such bubbles, featuring closed or recirculating streamlines, generally has depressed total pressure (and total pressure gradients) and represents a dispersed but contained region of vorticity. This is an example of an "imbedded" flow. The bubble is separated from the free stream by a strong shear layer (usually thin) surrounding it, so that the circulation calculated around any path within, or partially within, the bubble is not constrained in the usual way by Kelvin's theorem. The "core" of a tornado is another example of an imbedded flow of this type.

Generally, for strongly unsteady flows, key properties array themselves

on streaklines, not streamlines. Moreover, it is often difficult to perceive of, or even to properly define, "recirculating" streaklines. But in a well-developed vortex "street", certain patterns persist as they are convected along in the wake. It is then often possible to move into a reference frame, "convecting" with the pattern, in which the pattern appears to be steady, or only slowly-varying. In that case, in the new frame, streaklines and streamlines again become virtually coincident. It is then relatively easy to define, as in the case of the "bubble" above, imbedded, but convected, flow regions.

In a convecting vortex street pattern, well-defined regions of intense but dispersed vorticity, with corresponding entropy (or total pressure) variations appear and can be treated as "imbedded" flows, much as suggested above. The importance of this fact lies in the recirculating, or cyclic, feature of the flow viewed in the convecting frame. Because of the cyclic feature, some key properties of the convecting vorticity pattern can be deduced. In the following, we illustrate this feature for plane 2D flow.

The Cyclic Constraint - Vortex "Core" Properties

Our main interest in this Task is the development of concentrated, convecting vortex patterns in blade wakes at transonic Mach Nos. Compressibility and sound wave interaction can be important. But, in order to illustrate the cyclic constraint feature simply, we limit our discussion to the low Mach No. situation for the purposes of this report.

In the convecting frame, after the formation phase, the flow is nearly steady. The vorticity evolves in this phase according to the dissipative Helmholtz equation. At low Mach No. in plane 2D steady flow, this reduces to

$$q \frac{\partial}{\partial \ell} \Omega_z = \nu \nabla^2 \Omega_z \qquad (1)$$

where q is the fluid velocity in the convecting frame, $q \equiv |\underset{\sim}{q}|$, ν is the kinematic viscosity and Ω_z is the z-component of the vorticity, i.e., $\Omega_z \equiv (\text{curl } \underset{\sim}{q})\cdot\hat{e}_z$. "$\ell$" is a coordinate <u>along</u> a streamline (or streakline in the convecting frame).

If ψ is the streamfunction so that, with $\underset{\sim}{q} = (u,v)$

$$\left.\begin{aligned} \underset{\sim}{q} &= -\hat{e}_z \times \nabla\psi \\ q &= |\nabla\psi| \end{aligned}\right\} \tag{2}$$

then

$$\frac{\partial\psi}{\partial n} = q \tag{3}$$

and

$$\left(\frac{\partial v}{\partial x} - \frac{\partial u}{\partial y}\right) = \Omega_z = -\nabla^2\psi \tag{4}$$

Here, "n" is a coordinate <u>across</u> streamlines, orthogonal to "ℓ". "n" and "ℓ" make up the so-called "natural coordinates" often used in characteristic theory.

We can write

$$\Omega_z = f(\psi,\ell) \tag{5}$$

and note

$$\frac{\partial f}{\partial n} = f_\psi \psi_n = q f_\psi \tag{6}$$

where $f_\psi \equiv \partial f/\partial\psi$. We wish to find $f(\psi,\ell)$, or a good approximation to it, because if we can do that, we can determine the flow by solving

$$\nabla^2\psi = -f(\psi,\ell) \tag{7}$$

to determine $\psi(x,y)$.

Outside the thin shear layer surrounding the imbedded core of vorticity, we expect $f(\psi,\ell)$ to depend only weakly on "ℓ"; in fact, $\partial f/\partial\ell = O(\nu)$ from Eq. (1) unless $\nabla^2 f$ is itself very large. We note, accordingly,

$$\nabla f = f_\psi \nabla\psi + f_\ell \nabla\ell \doteq f_\psi \nabla\psi + O(\nu)$$

outside the shear layer, and

$$\nabla^2 f \doteq f_\psi \nabla^2\psi + f_{\psi\psi}|\nabla\psi|^2 + \ldots$$

in the same approximation. Thus,

$$\nabla^2 f \doteq -f f_\psi + q^2 f_{\psi\psi} \tag{8}$$

from Eqs. (5), (7) and (2), and Eq. (1) becomes

$$q \frac{\partial f}{\partial \ell} \doteq \nu\left(-f f_\psi + q^2 f_{\psi\psi}\right) \tag{9}$$

But, if the flow is imbedded, with cyclic properties, the integral around a recirculating streamline of $\partial f/\partial \ell$ must vanish. This yields the constraint

$$\oint d\ell \frac{\partial f}{\partial \ell} = 0 = \nu\left(-\oint f f_\psi \frac{d\ell}{q} + \oint f_{\psi\psi} q d\ell\right) \tag{10}$$

Thus, for any finite ν, no matter how small, the bracket in Eq. (10) must vanish. Equation (10) is limited to recirculating streamlines not in the shear layer.

Using the fact that f in this region is only weakly dependent on ℓ, the distance along the streamline, we can replace $f(\psi,\ell)$ by $F(\psi)$ in the integrals, obtaining approximately

$$0 \doteq -FF' \oint \frac{d\ell}{q} + F'' \oint q d\ell$$

or the constraint, for each ψ

$$F(\psi)F'(\psi) \doteq \frac{\Gamma(\psi)}{\tau(\psi)} F''(\psi) \tag{11}$$

where "Γ" is the circulation around the particular streamline, and "τ" is the corresponding "drift time":

$$\left.\begin{aligned} \tau &\equiv \oint \frac{d\ell}{q} \\ \Gamma &\equiv \oint q\,d\ell \end{aligned}\right\} \tag{12}$$

Ideas similar to these were put forward by Batchelor [1] years ago.

Application of the Cyclic Constraint

The usefulness of the constraint (Eq. (11)) can be seen readily when one realizes the simplicity of Γ and τ for a circular imbedded vortex core with centered solid-body rotation, $v_\theta = \omega_o r/2$, $\Omega_z = \omega_o$. In that simple case

$$\tau = \frac{4\pi}{\omega_o} = \text{const.} \tag{13}$$

$$\Gamma = \pi\omega_o r^2 = 4\pi\left(\psi - \psi_{min}\right) \tag{14}$$

(Solid body vortex.)

This suggests writing, in the general case of varying vorticity and a distorted (non-circular) imbedded region,

$$\frac{\Gamma}{\tau} = \omega_o\bar{\psi} + a\bar{\psi}^2 + b\bar{\psi}^3 + \ldots \tag{15}$$

where $\bar{\psi} = \psi - \psi_{min}$ and, correspondingly,

$$F(\psi) = \omega_o + A\bar{\psi} + B\bar{\psi}^2 + \ldots \tag{16}$$

Application of the constraint (Eq. (11)) then yields

$$a = 0\,, \quad A = 0$$

$$B = b$$

Thus, according to the constraint, no term linear in $\psi - \psi_{min}$ occurs in the vorticity.

Keeping only the above limited number of parameters, the internal recirculating flow is then determined by solving for ψ in the equation

$$-\nabla^2\psi = \omega_o + b\bar{\psi}^{-2} \quad . \tag{17}$$

While "ω_o" reflects the intensity of the internal flow, "b" emerges as a distortion parameter, reflecting the rearrangement of vorticity within and adjustment of the shape of the core, or bubble, as it interacts with the external flow, or free stream. Of course, more parameters, reflecting more details of the interaction, can be included, consistent with Eq. (11).

Extension of these ideas to higher Mach numbers introduces, of course, significant complexity due to compressibility but the basic usefulness of Eq. (11) or its generalization remains.

Variations from Radial Equilibrium

Use of the cyclic constraint above and the determination of the corresponding core flow in interaction with the external flow (and other "cores") will enable us to evaluate the effectiveness of earlier assumptions concerning radial equilibrium. With the correctly distorted core, an improved description of the momentum balance becomes available and more accurate descriptions of both the total temperature and entropy distributions are then possible.

Plans for Future Work

The ideas described above are being applied to the complex case of the wakes in a transonic compressor environment. 3D effects are to be included, using techniques indicated in earlier reports.

Reference

1. Batchelor, G.K., "On Steady Laminar Flow With Closed Streamlines at Large Reynolds Number," Journal of Fluid Mechanics, Vol. 1, 1956, p. 177.

3. PUBLICATIONS AND PRESENTATIONS

W.F. Ng and A.H. Epstein, "A Quasi-Three-Dimensional Model for Intra-Stator Transport of Rotor Wakes," submitted to ASME Journal (presented at ASME Winter Annual Meeting, November 1985).

E.M. Greitzer, "Flow Instabilities in Turbomachines," Review Article in Thermodynamics and Fluid Mechanics of Turbomachinery, Martinus Nijhoff Publishers (proceedings of NATO Advanced Study Institute), January 1986.

H.W. Shin, E.M. Greitzer, W.K. Cheng, C.S. Tan, and C.L. Shippee, "Circulation Measurements and Vortical Structure in an Inlet Vortex Flow Field," Journal of Fluid Mechanics, Vol. 162, January 1986, pp. 463-487.

C.S. Tan and E.M. Greitzer, "Compressible Swirling Flow in Turbomachine Annuli," AIAA Journal, Vol. 24, No. 1, January 1986, pp. 92-101.

H.W. Shin, W.K. Cheng, E.M. Greitzer, and C.S. Tan, "Inlet Vortex Formation due to Ambient Vorticity Intensification," AIAA Journal, Vol. 24, No. 4, April 1986, p. 687.

M. Drela and M. Giles, "Viscous-Inviscid Analysis of Transonic and Low Reynolds Number Airfoils," AIAA-86-1786-CP, presented at the AIAA 4th Applied Aerodynamics Conference, June 9-11, 1986.

M. Giles and M. Drela, "A Two-Dimensional Transonic Aerodynamic Design Method," AIAA-86-1793-CP, presented at the AIAA 4th Applied Aerodynamics Conference, June 9-11, 1986.

A.H. Epstein, J.B. Gertz, P.R. Owen and M.B. Giles, "Vortex Shedding in Compressor Blade Wakes," presented at AGARD/PEP Specialist Meeting, Munich, Germany, September 1986; also submitted to AIAA J. of Propulsion and Power.

M. Drela and M. Giles, contributed paper to Viscous Transonic Airfoil Workshop, to be presented at the AIAA 25th Aerospace Sciences Meeting, January 12-15, 1987.

M.C. Johnson and E.M. Greitzer, "Effects of Slotted Hub and Casing Treatments on Compressor Endwall Flow Fields," presented at 1986 ASME International Gas Turbine Conference, Dusseldorf, Germany, June 1986; also to be published in ASME J. Eng. Gas Turbines and Power.

C.S. Tan, "A Mixed Spectral-Finite Difference Scheme for Three-Dimensional Viscous Flow in a Bend of Rectangular Cross-Section," submitted to Journal of Computational Physics.

M. Kurosaka, J. Gertz, J.E. Graham, W.L. Hankey, and P. Sundown, "Energy Separation in a Vortex Street, Part II: The Mechanism," to be published in Journal of Fluid Mechanics.

M. Giles and M. Drela, Two-Dimensional Aerodynamic Design and Analysis, to be published by Cambridge University Press in 1987.

4. PROGRAM PERSONNEL

Principal Investigator:

Edward M. Greitzer
Professor of Aeronautics and Astronautics
Director, Gas Turbine Laboratory

Co-Investigators:

Alan H. Epstein
Associate Professor of Aeronautics and Astronautics
Associate Director, Gas Turbine Laboratory

Michael B. Giles
Assistant Professor of Aeronautics and Astronautics

James E. McCune
Professor of Aeronautics and Astronautics

Choon S. Tan
Research Associate

Graduate Research Assistants (total contract period):

9/83 - 1/85	Mark Johnson (AFRAPT Student)*, "Effects of Hub Treatment on Compressor Endwall Flow Fields" (thesis title)
9/81 - 6/85	Thong Dang**, "A Two-Dimensional Design Method for Highly-Loaded Blades in Turbomachines" (thesis title)
9/83 - Present	Petros Kotidis*, "Investigation of the Radial Transport in a Transonic Compressor Rotor Stage" (thesis title)
9/83 - 10/85	Mark Drela**, "Two-Dimensional Transonic Aerodynamic Design and Analysis Using the Euler Equations" (thesis title)
9/83 - 6/85	Michael Giles**, "Newton Solution of Steady Two Dimensional Transonic Flow" (thesis title)
9/84 - 9/86	Phil Owen*, "Computational Simulation of Unsteady Flow in a Transonic Compressor Rotor" (thesis title)
9/84 - Present	Norman Lee
9/85 - Present	Edward Imperatori
9/86 - Present	S. Allmaras (AFRAPT student)

* S.M. Degree Completed
**Ph.D Thesis Completed

5. INTERACTIONS

There are considerable interactions between Gas Turbine Laboratory personnel and industry and government. Listed below are only those which involved discussions of AFOSR projects. It should be noted that a considerable amount of the research at the GTL is supported by the aircraft engine industry and this promotes a large amount of technical interaction between MIT and the sponsors.

Seminars and Technical Discussions

Technical discussions between A.H. Epstein and AFWAL personnel on Rotating Turbine Design and Research, ongoing 1986.

Presentation by C.S. Tan on "Spectral Methods for Flow in Turbomachinery" at Princeton University, January 1986.

Presentation by C.S. Tan on "Spectral Methods for Internal Flow" at Los Alamos National Laboratory, May 1986.

Seminar by E.M. Greitzer on "Mechanisms of [illegible] Treatment [illegible] ment" at Allison Gas Turbine [illegible], [illegible] 1986.

Presentation by [illegible] on "[illegible] Flow [illegible] Transonic Compressor [illegible] at [illegible] Turbine [illegible] 1986.

Presentation by E.M. [illegible] "[illegible] MIT [illegible] Laboratory" at [illegible] Turbine [illegible] Company [illegible]

[illegible] by E.M. [illegible] Turbine Laboratory [illegible]

[illegible]

The Gas Turbine Laboratory also has an active seminar program to increase interaction with industry and/or government by bringing speakers to MIT. During the period covered by this report, these have included:

Mr. [illegible] Sharma, Pratt & Whitney Aircraft
"Turbine Losses"

Dr. W. Steenken, General Electric Company
"Stall Phenomena in Multistage Compressors"

Mr. R. Sellers, Pratt & Whitney Aircraft
"[illegible] Aero-Thermodynamics"

Dr. [illegible] Weber, Cummins Engine Company
"Modern Problems in Turbocharger Fluid Mechanics"

Mr. [illegible] w, Pratt & Whitney Aircraft
"Planning a New Engine - From Blank Piece of Paper [illegible]"

Dr. A. F. Ferri, Aerojet Gas Turbine Division, G.M. Corp.
"[illegible]"

6. DISCOVERIES, INVENTIONS, AND SCIENTIFIC APPLICATIONS

During the present contract period, there have been no inventions.

7. CONCLUDING REMARKS

We feel that the multi-investigator format has been very successful in its application at MIT. One facet of this has been the flexibility to assign resources among the individual projects. Another, perhaps more important, aspect has been the interactions that have developed between various investigators. We will give just two examples of such interactions. As one, Professors Epstein and Greitzer (plus personnel from our Guidance and Control Division) are starting a new multi-disciplinary research area, involving theoretical and experimental investigation of suppression of turbomachinery instabilities by active control. As a second, Phil Owen, a student of Epstein's, was able to use Giles' unsteady Navier-Stokes code to examine a phenomenon that had been seen experimentally. This latter type of interaction, where state-of-the-art computer codes are used to derive a new quantitative appreciation for phenomena (rather than merely run as design tools) seems to us to be at the core of this type of multi-investigator research program. A necessary (although not sufficient) condition for it to exist is the existence of a critical mass of faculty, staff and students who are interested in the type of complex problems that characterize high performance engines, and we hope that the Gas Turbine Laboratory can continue to receive support to maintain such an effort.

END

3-87

DTIC